25. Bligh, E.G., and Dyer, W. J. (1959) A rapid method of total lipid extraction and purification. *Can. J. Biochem. Physiol.* **37,** 911–917
26. Pettus, B. J., Bielawski, J., Porcelli, A. M., Reames, D. L., Johnson, K. R., Morrow, J., Chalfant, C. E., Obeid, L. M., and Hannun, Y. A. (2003) The sphingosine kinase 1/sphingosine-1-phosphate pathway mediates COX-2 induction and PGE_2 production in response to TNF-α. *FASEB J.* **17,** 1411–1421
27. Gonzalez, A. A., Kumar, R., Mulligan, J. D., Davis, A. J., Weindruch, R., and Saupe, K. W. (2004) Metabolic adaptations to fasting and chronic caloric restriction in heart, muscle, and liver do not include changes in AMPK activity. *Am. J. Physiol. Endocrinol. Metab.* **287,** E1032–E1037
28. Wojtaszewski, J. F., Jorgensen, S. B., Hellsten, Y., Hardie, D. G., and Richter, E. A. (2002) Glycogen-dependent effects of 5-aminoimidazole-4-carboxamide (AICA)-riboside on AMP-activated protein kinase and glycogen synthase activities in rat skeletal muscle. *Diabetes* **51,** 284–292
29. Zang, M., Zuccollo, A., Hou, X., Nagata, D., Walsh, K., Herscovitz, H., Brecher, P., Ruderman, N. B., and Cohen, R. A. (2004) AMP-activated protein kinase is required for the lipid-lowering effect of metformin in insulin-resistant human HepG2 cells. *J. Biol. Chem.* **279,** 47898–47905
30. Grassme, H., Gulbins, E., Brenner, B., Ferlinz, K., Sandhoff, K., Harzer, K., Lang, F., and Meyer, T. F. (1997) Acidic sphingomyelinase mediates entry of *N. gonorrhoeae* into nonphagocytic cells. *Cell* **91,** 605–615
31. Pyne, S., and Pyne, N. J. (2002) Sphingosine 1-phosphate signalling and termination at lipid phosphate receptors. *Biochim. Biophys. Acta* **1582,** 121–131
32. Olivera, A., and Spiegel, S. (1993) Sphingosine-1-phosphate as second messenger in cell proliferation induced by PDGF and FCS mitogens. *Nature* **365,** 557–560
33. Siehler, S., and Manning, D. R. (2002) Pathways of transduction engaged by sphingosine 1-phosphate through G protein-coupled receptors. *Biochim. Biophys. Acta* **1582,** 94–99
34. Yang, A. H., Ishii, I., and Chun, J. (2002) In vivo roles of lysophospholipid receptors revealed by gene targeting studies in mice. *Biochim. Biophys. Acta* **1582,** 197–203
35. Hardie, D. G. (2007) AMP-activated/SNF1 protein kinases: conserved guardians of cellular energy. *Nat. Rev. Mol. Cell Biol.* **8,** 774–785
36. Leclerc, I., Lenzner, C., Gourdon, L., Vaulont, S., Kahn, A., and Viollet, B. (2001) Hepatocyte nuclear factor-4α involved in type 1 maturity-onset diabetes of the young is a novel target of AMP-activated protein kinase. *Diabetes* **50,** 1515–1521
37. Hou, X., Xu, S., Maitland-Toolan, K. A., Sato, K., Jiang, B., Ido, Y., Lan, F., Walsh, K., Wierzbicki, M., Verbeuren, T. J., Cohen, R. A., and Zang, M. (2008) SIRT1 regulates hepatocyte lipid metabolism through activating AMP-activated protein kinase. *J. Biol. Chem.* **283,** 20015–20026
38. Wu, Y., Song, P., Xu, J., Zhang, M., and Zou, M. H. (2007) Activation of protein phosphatase 2A by palmitate inhibits AMP-activated protein kinase. *J. Biol. Chem.* **282,** 9777–9788
39. Igarashi, J., Shoji, K., Hashimoto, T., Moriue, T., Yoneda, K., Takamura, T., Yamashita, T., Kubota, Y., and Kosaka, H. (2009) Transforming growth factor-β1 down-regulates caveolin-1 expression and enhances sphingosine 1-phosphate signaling in cultured vascular endothelial cells. *Am. J. Physiol. Cell Physiol* **297,** C1263–C1274
40. Adams, J. M., 2nd, Pratipanawatr, T., Berria, R., Wang, E., DeFronzo, R. A., Sullards, M. C., and Mandarino, L. J. (2004) Ceramide content is increased in skeletal muscle from obese insulin-resistant humans. *Diabetes* **53,** 25–31
41. Glimcher, L. H., and Lee, A. H. (2009) From sugar to fat: How the transcription factor XBP1 regulates hepatic lipogenesis. *Ann. N. Y. Acad. Sci.* **1173**(Suppl. 1), E2–E9
42. Stiles, B., Wang, Y., Stahl, A., Bassilian, S., Lee, W. P., Kim, Y.-J., Sherwin, R., Devaskar, S., Lesche, R., Magnuson, M. A., and Wu, H. (2004) Live-specific deletion of negative regulator Pten results in fatty liver and insulin hypersensitivity. *Proc. Natl. Acad. Sci. U. S. A.* **101,** 2082–2087
43. Watson, R. T., Shigematsu, S., Chiang, S. H., Mora, S., Kanzaki, M., Macara, I. G., Saltiel, A. R., and Pessin, J. E. (2001) Lipid raft microdomain compartmentalization of TC10 is required for insulin signaling and GLUT4 translocation. *J. Cell Biol.* **154,** 829–840
44. Sebastian, B. M., and Nagy, L. E. (2005) Decreased insulin-dependent glucose transport by chronic ethanol feeding is associated with dysregulation of the Cbl/TC10 pathway in rat adipocytes. *Am. J. Physiol. Endocrinol. Metab.* **289,** E1077–E1084
45. Zeidan, Y. H., and Hannun, Y. A. (2010) The acid sphingomyelinase/ceramide pathway: biomedical significance and mechanisms of regulation. *Curr. Mol. Med.* **10,** 454–466

Received for publication July 23, 2010.
Accepted for publication December 2, 2010.

ARTICLE

Journal of Cellular Biochemistry 112:949–953 (2011)

Journal of Cellular Biochemistry

Imaging the Recruitment of Cancer-Associated Fibroblasts by Liver-Metastatic Colon Cancer

Atsushi Suetsugu,[1,2,3] Yosuke Osawa,[3] Masahito Nagaki,[3] Shigetoyo Saji,[4] Hisataka Moriwaki,[3] Michael Bouvet,[1] and Robert M. Hoffman[1,2*]

[1] *AntiCancer, Inc., San Diego, California 92111*

[2] *Department of Surgery, University of California, San Diego, California 92103*

[3] *Department of Gastroenterology, Gifu University Graduate School of Medicine, Gifu, Japan*

[4] *Department of Surgical Oncology, Gifu University Graduate School of Medicine, Gifu, Japan*

ABSTRACT

The tumor microenvironment (TME) is critical for tumor growth and progression. However, the formation of the TME is largely unknown. This report demonstrates a color-coded imaging model in which the development of the TME can be visualized. In order to image the TME, a green fluorescent protein (GFP)-expressing mouse was used as the host which expresses GFP in all organs but not the parenchymal cells of the liver. Non-colored HCT-116 human colon cancer cells were injected in the spleen of GFP nude mice which led to the formation of experimental liver metastasis. TME formation resulting from the liver metastasis was observed using the Olympus OV100 small animal fluorescence imaging system. HCT-116 cells formed tumor colonies in the liver 28 days after cell transplantation to the spleen. GFP-expressing host cells were recruited by the metastatic tumors as visualized by fluorescence imaging. A desmin positive area increased around and within the liver metastasis over time, suggesting cancer-associated fibroblasts (CAFs) were recruited by the liver metastasis which have a role in tumor progression. The color-coded model of the TME enables its formation to be visualized at the cellular level in vivo, in real-time. This imaging model of the TME should lead to new visual targets in the TME. J. Cell. Biochem. 112: 949–953, 2011. © 2010 Wiley-Liss, Inc.

KEY WORDS: GFP AND RFP NUDE MICE; TUMOR MICROENVIRONMENT; STROMAL CELLS; CANCER-ASSOCIATED FIBROBLASTS; LIVER METASTASIS; COLOR-CODED IMAGING

The use of fluorescent proteins for imaging is revolutionizing in vivo biology [Hoffman, 2005, 2008]. Green fluorescent protein (GFP) and red fluorescent protein (RFP) have been shown to be able to be genetically linked with almost any protein providing a permanent and heritable label in live cells to study protein function and location. Many different colors of fluorescent proteins have now been produced in the laboratory or found in nature [Matz et al., 1999; Shaner et al., 2004]. With different color fluorescent proteins, many processes can be visualized simultaneously in cells. Thus, live cells can be multiply labeled for imaging processes that heretofore could be seen only on fixed and stained cells. The use of fluorescent proteins for imaging in vivo has been particularly useful to study tumor growth and progression [Hoffman, 2005].

With the use of multiple colored-proteins, we developed imaging of the tumor microenvironment (TME) by color-coding cancer and stromal cells. The TME is critical for tumor growth and progression. Indeed, cancer cells and stromal cells must replicate in parallel in order for the tumor to grow. Our original color-coded imaging technology of the TME used a GFP or RFP transgenic nude mouse as a host in which we transplanted cancer cells expressing a fluorescent protein not expressed by the host [Yang et al., 2003, 2004, 2009].

Recently, color-coded in vivo imaging has shown that stromal cells had higher motility in the microenvironment at the tumor periphery than within the tumor mass [Egeblad et al., 2008]. Solid tumors contain fibroblasts, lymphocytes, dendritic, macrophages, and other myeloid cells in their microenvironment [Egeblad et al., 2008].

Myofibroblasts and are a major population of carcinoma-associated fibroblasts (CAFs) [Kalluri and Zeisberg, 2006]. CAFs stimulate cancer cell growth, inflammation, angiogenesis, and invasion [Kalluri and Zeisberg, 2006; Gaggioli et al., 2007; Pietras

Abbreviations used: TME, tumor microenvironment; GFP, green fluorescent protein; RFP, red fluorescent protein; CAF, cancer-associated fibroblasts.

*Correspondence to: Robert M. Hoffman, PhD, AntiCancer, Inc., 7917 Ostrow Street, San Diego, CA 92111. E-mail: all@anticancer.com

Received 16 December 2010; Accepted 20 December 2010 • DOI 10.1002/jcb.23011 • © 2010 Wiley-Liss, Inc.

Published online 29 December 2010 in Wiley Online Library (wileyonlinelibrary.com).

et al., 2008; Erez et al., 2010]. As the tumor grows, it recruits CAFs [Orimo et al., 2005; Egeblad et al., 2010].

How the TME is formed in real time during cancer progression is not known. The present study utilizes color-coded fluorescent protein-based imaging to visualize the recruitment over time of stromal cells including CAFs by liver metastases of the colon cancer.

MATERIALS AND METHODS

CELL CULTURE

The HCT-116 human colon cancer cell line was originally obtained from the American Type Culture Collection (Manassas, VA). The cells were maintained in RPMI 1640 supplemented with 10% FCS. All media were supplemented with penicillin and streptomycin (Gibco BRL). The cell line was cultured at 37°C in a 5% incubator.

GFP TRANSGENIC MICE

Transgenic C57/B6-GFP mice [Okabe et al., 1997] were obtained from the Research Institute for Microbial Diseases (Osaka University, Osaka, Japan). The C57/B6-GFP mice expressed the *Aequorea victoria* GFP under the control of the chicken β-actin promoter and cytomegalovirus enhancer. The GFP gene was crossed into nude mice on the C57/B6 background [Yang et al., 2004]. Transgenic C57/B6-RFP mice were obtained from Jackson Labs (Bar Harbor, ME). C57/B6-RFP mice expressed the RFP (DsREDT3) under the control of a chicken β-actin promoter and cytomegalovirus enhancer [Vintersten et al., 2004]. The RFP gene was crossed into nude mice (Harlan, Indianapolis, IN) on the BALB/c and NCR background [Yang et al., 2009]. All animal studies were conducted in accordance with the principles of and procedures outlined in the NIH guide for the care and use of laboratory animals under assurance number A3873-1.

NON-COLORED COLON CANCER CELL (HCT-116)-GFP HOST MODEL

Six-week-old GFP nude mice were used as the host for non-colored HCT-116 human colon cancer cells. Non-colored HCT-116 cells were first harvested by trypsinization and washed three times with cold serum-free medium and then resuspended with serum-free RPMI 1640 medium. GFP nude mice were anesthetized with a ketamine mixture (10 μl ketamine HCl, 7.6 μl xylazine, 2.4 μl acepromazine maleate, and 10 μl H_2O) injected into the peritoneal cavity. Non-colored human HCT-116 colon cancer cells (2.0×10^6) were injected in the spleen of GFP nude mice during open laparotomy in order for experimental liver metastases to form.

IN VIVO IMAGING

For in vivo imaging based on fluorescent proteins [Hoffman, 2005; Hoffman and Yang, 2006a,b,c], the Olympus OV100 Small Animal Imaging System (Olympus Corp., Tokyo, Japan) was used. The Olympus OV100, which contains an MT-20 light source (Olympus Biosystems, Planegg, Germany) and DP70 CCD camera (Olympus), was used for cellular imaging in live mice. The optics of the OV100 fluorescence imaging system have been specially developed for macro-imaging as well as micro-imaging with high light-gathering capacity. The instrument incorporates a unique combination of high numerical aperture and long working distance. Four individually optimized objective lenses, parcentered and parfocal, provide a 10^5-fold magnification range for seamless imaging of the entire body down to the subcellular level without disturbing the animal. The OV100 has the lenses mounted on an automated turret with a high magnification range of 1.6× to 16× and a field of view ranging from 6.9 to 0.69 mm. The optics and antireflective coatings ensure optimal imaging of multiplexed fluorescent reporters in small animals. High-resolution images were captured directly on a PC (Fujitsu Siemens, Munich, Germany). Images were processed for contrast and brightness and analyzed with the use of Paint Shop Pro 8 and Cell^R (Olympus Biosystems) [Yamauchi et al., 2006].

HISTOLOGICAL ANALYSIS

The host livers were fixed with 10% buffered formalin, sectioned at a thickness of 4 μm, and stained with hematoxylin and eosin. The fluorescent cell area was measured using the National Institutes of Health (NIH) Image analysis software program (available at http://rsb.info.nih.gov/nih-image/). Desmin was stained with anti-desmin antibody (Lab Vision, Fremont, CA) using avidin–biotin–peroxidase complex technique (Vector, Burlingame, CA). Measurement of positive area was performed using the NIH Image.

STATISTICAL ANALYSIS

All data represent the mean of at least three independent experiments ± SD. For the determination of statistical significance, unpaired Student's *t*-tests were performed. *P*-values of less than 0.01 were considered statistically significant.

RESULTS AND DISCUSSION

FLUORESCENT ORGANS IN GFP AND RFP NUDE MICE

After sacrifice of the GFP and RFP transgenic nude mice, organs including lungs (Fig. 1A), kidney (Fig. 1B), esophagus (Fig. 1C), stomach (Fig. 1C), duodenum (Fig. 1C), small intestines (Fig. 1D), colon (Fig. 1D), the circulatory system, uterus and ovary, pancreas, brain, heart, and spleen (data not shown) were harvested, and imaged with the Olympus OV100 Small Animal Imaging System. All of the tissues from the RFP transgenic mouse, with the exception of erythrocytes, were red fluorescent under appropriate excitation light (Fig. 1). In contrast, although the other organs of the GFP-transgenic nude mice were brightly fluorescent, the liver of GFP nude mice fluorescence was weak except for the gallbladder (Fig. 1E).

IMAGING RECRUITMENT OF CANCER-ASSOCIATED FIBROBLASTS BY COLON CANCER LIVER METASTASIS

Human non-colored HCT-116-colon cancer cells were injected in the spleen of GFP nude mice. On day 28 after cancer-cell injection, GFP fluorescence was observed in the experimental liver metastatic colonies. High-magnification fluorescence microscopy showed extensive GFP fluorescence in the tumor. Liver sections were stained with hematoxylin–eosin, and GFP fluorescence of recruited GFP-expressing hosts cells in the liver metastasis was observed. There was a very large increase of GFP expression in the tumor compared to the non-tumor-bearing liver in nude mice. There was also significantly more GFP fluorescence in the liver metastasis

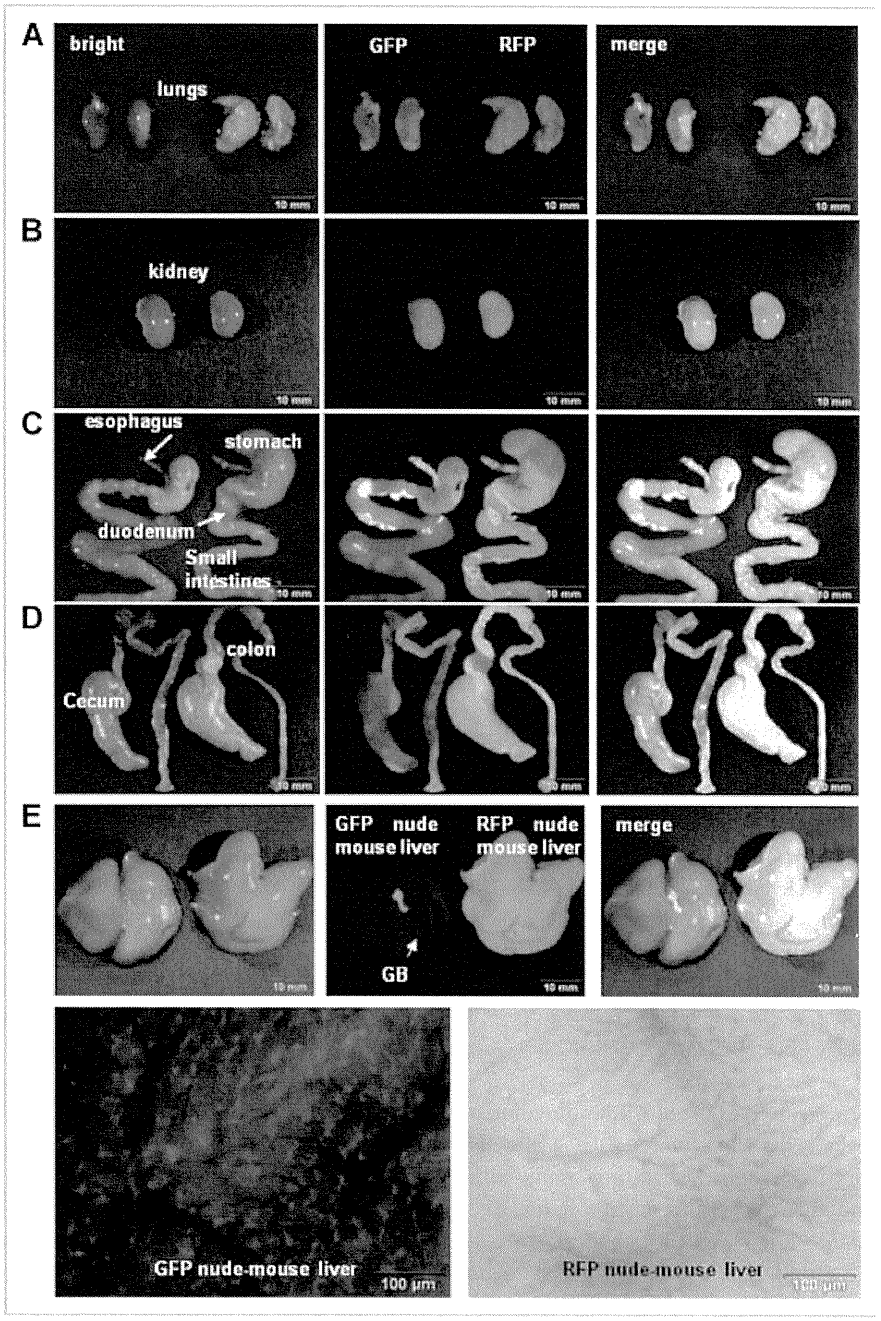

Fig. 1. Major organs of transgenic GFP and RFP nude mice. Fluorescence of organs after excitation with blue light. A: Lungs; (B) kidney; (C,D) digestive tract; (E) liver. Lower panel displayed high magnification (16×). The liver of GFP nude mice has very weak fluorescence.

compared to the non-tumor area of the liver ($P < 0.01$). Thus, the host GFP cells were imaged extensively accumulating in the liver metastasis. Expression of desmin was determined by immunohistochemistry with anti-desmin antibody and found to be positive in the tumor area. Thus, the liver metastasis contained GFP- and desmin-expressing cells, suggesting that cancer-associated fibroblasts (CAFs) were recruited and grew in the tumor (Fig. 2).

It is well known that CAFs have an important role in tumor progression [Erez et al., 2010]. CAFs have an increased rate of proliferation and differential expression of extracellular matrix (ECM) components and growth factors compared to normal fibroblasts [Bhowmick et al., 2004; Kalluri and Zeisberg, 2006; Erez et al., 2010]. CAFs promote tumor growth by inducing angiogenesis, recruiting bone marrow-derived endothelial progenitor cells, and remodeling the ECM [Olumi et al., 1999; Allinen et al., 2004; Orimo et al., 2005; Pietras et al., 2008; Erez et al., 2010]. CAFs can confer resistance to antiangiogenic therapy [Crawford et al., 2009; Erez et al., 2010]. CAFs also mediate tumor-enhancing inflammation mediated by NF-kappaB signaling [Erez et al., 2010].

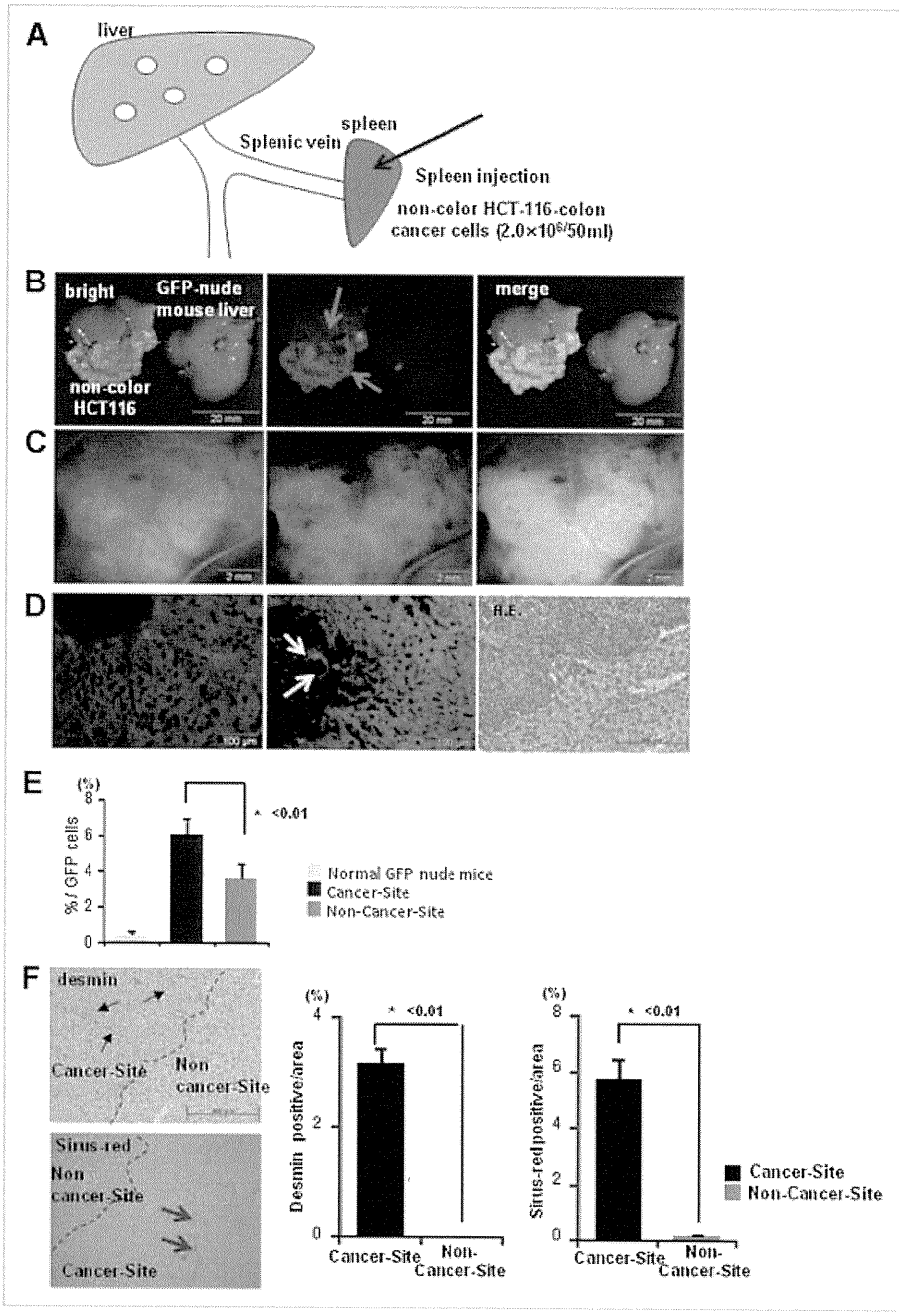

Fig. 2. Tumor–host interaction of non-colored human colon tumors in the liver of GFP nude mice. A: Schematic representation of experimental protocol. Human non-colored HCT-116-colon cancer cells (2.0×10^6/50 μl) were injected in the spleen of GFP nude mice during open laparotomy. B: On day 28 after cancer-cell injection, GFP fluorescence was observed in the liver metastasis (red arrows; left panel: bright field; central panel: fluorescence; right panel: merge; original magnification 0.14×). C: High magnification (left panel: bright-field; central panel: fluorescence; right panel: merge). D: Liver sections from GFP nude mice were stained with hematoxylin–eosin, and GFP fluorescence of non-parenchymal cells in the host GFP liver was observed as well (yellow arrows). E: There was significantly more GFP fluorescence in the metastasis than in the non-tumor part of the liver ($P < 0.01$). F: Expression of desmin was determined by immunohistochemistry with anti-desmin antibody (arrows; original magnification 100×). Measurement of the desmin-positive area was performed using the NIH Image analysis software program. Data are means ± SD from three independent experiments. Collagen deposition was assessed by Sirus red staining (blue arrows). The host GFP non-parenchymal cells were observed in the experimental liver metastasis. Non-parenchymal cells accumulated in tumors compared with normal liver. Liver metastasis contained GFP and desmin-expressing cells, suggesting that cancer-associated fibroblast cells have a role in metastasis.

The present report enables imaging of accumulation of CAFs of the tumor in real time.

The TME is critical for tumor growth and progression. However, the formation of the TME is largely unknown. This report demonstrates a color-coded imaging model in which the development of the TME can be visualized. In the GFP transgenic nude mice, only non-parenchymal cells of the liver have GFP fluorescence, which makes it a very useful model to image stromal development in the tumor, since GFP-expressing stromal cells were recruited by the metastatic tumors. A desmin-positive area increased around the

liver metastatic tumors over time, suggesting CAFs were recruited by the metastatic tumors and have an important role in tumor progression. Stromal cells essential for metastatic tumors to develop in the liver can be identified with the stromal imaging model described in this report.

REFERENCES

Allinen M, Beroukhim R, Cai L, Brennan C, Lahti-Domenici J, Huang H, Porter D, Hu M, Chin L, Richardson A, Schnitt S, Sellers WR, Polyak K. 2004. Molecular characterization of the tumor microenvironment in breast cancer. Cancer Cell 6:17–32.

Bhowmick NA, Neilson EG, Moses HL. 2004. Stromal fibroblasts in cancer initiation and progression. Nature 432:332–337.

Crawford Y, Kasman I, Yu L, Zhong C, Wu X, Modrusan Z, Kaminker J, Ferrara N. 2009. PDGF-C mediates the angiogenic and tumorigenic properties of fibroblasts associated with tumors refractory to anti-VEGF treatment. Cancer Cell 15:21–34.

Egeblad M, Ewald AJ, Askautrud HA, Truitt ML, Welm BE, Bainbridge E, Peeters G, Krummel MF, Werb Z. 2008. Visualizing stromal cell dynamics in different tumor microenvironments by spinning disk confocal microscopy. Dis Model Mech 1:155–167.

Egeblad M, Nakasone ES, Werb Z. 2010. Tumors as organs: Complex tissues that interface with the entire organism. Dev Cell 18:884–901.

Erez N, Truitt M, Olson P, Arron ST, Hanahan D. 2010. Cancer-associated fibroblasts are activated in incipient neoplasia to orchestrate tumor-promoting inflammation in an NF-kappaB-dependent manner. Cancer Cell 17:135–147.

Gaggioli C, Hooper S, Hidalgo-Carcedo C, Grosse R, Marshall JF, Harrington K, Sahai E. 2007. Fibroblast-led collective invasion of carcinoma cells with differing roles for RhoGTPases in leading and following cells. Nat Cell Biol 9:1392–1400.

Hoffman RM. 2005. The multiple uses of fluorescent proteins to visualize cancer in vivo. Nat Rev Cancer 5:796–806.

Hoffman RM. 2008. A better fluorescent protein for whole-body imaging. Trends Biotechnol 26:1–4.

Hoffman RM, Yang M. 2006a. Subcellular imaging in the live mouse. Nat Protoc 1:775–782.

Hoffman RM, Yang M. 2006b. Color-coded fluorescence imaging of tumor-host interactions. Nat Protoc 1:928–935.

Hoffman RM, Yang M. 2006c. Whole-body imaging with fluorescent proteins. Nat Protoc 1:1429–1438.

Kalluri R, Zeisberg M. 2006. Fibroblasts in cancer. Nat Rev Cancer 6:392–401.

Matz MV, Fradkov AF, Labas YA, Savitsky AP, Zaraisky AG, Markelov ML, Lukyanov SA. 1999. Fluorescent proteins from nonbioluminescent Anthozoa species. Nat Biotechnol 17:969–973.

Okabe M, Ikawa M, Kominami K, Nakanishi T, Nishimune Y. 1997. 'Green mice' as a source of ubiquitous green cells. FEBS Lett 407:313–319.

Olumi AF, Grossfeld GD, Hayward SW, Carroll PR, Tlsty TD, Cunha GR. 1999. Carcinoma-associated fibroblasts direct tumor progression of initiated human prostatic epithelium. Cancer Res 59:5002–5011.

Orimo A, Gupta PB, Sgroi DC, Arenzana-Seisdedos F, Delaunay T, Naeem R, Carey VJ, Richardson AL, Weinberg RA. 2005. Stromal fibroblasts present in invasive human breast carcinomas promote tumor growth and angiogenesis through elevated SDF-1/CXCL12 secretion. Cell 121:335–348.

Pietras K, Pahler J, Bergers G, Hanahan D. 2008. Functions of paracrine PDGF signaling in the proangiogenic tumor stroma revealed by pharmacological targeting. PLoS Med 5:e19.

Shaner NC, Campbell RE, Steinbach PA, Giepmans BN, Palmer AE, Tsien RY. 2004. Improved monomeric red, orange and yellow fluorescent proteins derived from Discosoma sp. red fluorescent protein. Nat Biotechnol 22:1567–1572.

Vintersten K, Monetti C, Gertsenstein M, Zhang P, Laszlo L, Biechele S, Nagy A. 2004. Mouse in red: Red fluorescent protein expression in mouse ES cells, embryos, and adult animals. Genesis 40:241–246.

Yamauchi K, Yang M, Jiang P, Xu M, Yamamoto N, Tsuchiya H, Tomita K, Moossa AR, Bouvet M, Hoffman RM. 2006. Development of real-time subcellular dynamic multicolor imaging of cancer-cell trafficking in live mice with a variable-magnification whole-mouse imaging system. Cancer Res 66:4208–4214.

Yang M, Li L, Jiang P, Moossa AR, Penman S, Hoffman RM. 2003. Dual-color fluorescence imaging distinguishes tumor cells from induced host angiogenic vessels and stromal cells. Proc Natl Acad Sci USA 100:14259–14262.

Yang M, Reynoso J, Jiang P, Li L, Moossa AR, Hoffman RM. 2004. Transgenic nude mouse with ubiquitous green fluorescent protein expression as a host for human tumors. Cancer Res 64:8651–8656.

Yang M, Reynoso J, Bouvet M, Hoffman RM. 2009. A transgenic red fluorescent protein-expressing nude mouse for color-coded imaging of the tumor microenvironment. J Cell Biochem 106:279–284.

MOLECULAR CANCER

RESEARCH Open Access

Dual induction of caspase 3- and transglutaminase-dependent apoptosis by acyclic retinoid in hepatocellular carcinoma cells

Hideki Tatsukawa[1], Tetsuro Sano[2], Yayoi Fukaya[1], Naoto Ishibashi[3], Makiko Watanabe[3], Masataka Okuno[4], Hisataka Moriwaki[4], Soichi Kojima[1*]

Abstract

Background: Hepatocellular carcinoma has a high mortality rate due to its rate of recurrence. Acyclic retinoid prevents recurrence of hepatocellular carcinoma in patients after surgical removal of their primary tumors by inducing apoptosis in hepatocellular carcinoma cells, although the molecular mechanisms of action are not understood.

Methods: Human hepatocellular carcinoma cells in culture, as well as nude mice transplanted with hepatocellular carcinoma cells and rats given with *N*-diethylnitrosamine were treated with acyclic retinoid. Changes in activated caspase 3 and transglutaminase 2 (TG2) levels, Sp1 cross-linking and its activities, expression of epidermal growth factor receptor, and apoptotic levels were measured.

Results: Acyclic retinoid simultaneously stimulated the activation of caspase 3, and the expression, nuclear localization and crosslinking activity of TG2, resulting in crosslinking and inactivation of the transcription factor, Sp1, thereby reducing expression of epidermal growth factor receptor and cell death in three hepatocellular carcinoma cell lines. These effects were partially restored by a caspase inhibitor, transfection of antisense TG2, restoration of functional Sp1, or an excess of epidermal growth factor. Nuclear expression of TG2 and crosslinked Sp1, as also activated caspase 3 were found in both hepatocellular carcinoma cells transplanted into nude mice and cancerous regions within the liver in *N*-diethylnitrosamine-induced hepatocarcinogenesis model in rats, following treatment of animals with acyclic retinoid.

Conclusions: Treatment with acyclic retinoid produces a dual activation of caspase 3 and TG2 induced apoptosis of hepatocellular carcinoma cells via modification and inactivation of Sp1, resulting in reduced expression of epidermal growth factor receptor.

Background

Hepatocellular carcinoma (HCC) has high mortality rate because of it frequent rate of recurrence [1]. Acyclic retinoid (ACR), a synthetic retinoid, prevents the recurrence and development of HCC in patients after surgical removal of the primary tumors by inducing apoptosis in HCC cells [2,3]. Retinoid X receptor (RXR) α is highly phosphorylated and loses its activity as a transcriptional factor during carcinogenesis in HCC [4]. ACR prevents this aberrant hyper-phosphorylation of RXRα by suppressing the Ras-extracellular signal regulated kinase (Erk) pathway, thereby restoring RXRα's activity in response to physiological concentrations of 9-*cis* retinoic acid (9-*cis* RA) [5]. We therefore proposed that this restoration of RXRα transcriptional activity is a basis for ACR's activity to control aberrant cell growth and induce apoptosis. However, the possibility that genes under the control of RARα/RXRv are upregulated by

* Correspondence: skojima@riken.jp
[1]Molecular Ligand Biology Research Team, Chemical Genomics Research Group, Chemical Biology Department, RIKEN Advanced Science Institute, Wako, Saitama 351-0198, Japan
Full list of author information is available at the end of the article

ACR, thereby mediating ACR's effect in suppressing aberrant growth and/or inducing apoptosis, has not been fully elucidated. ACR downregulates epidermal growth factor receptor (EGFR) signals due to suppression of transforming growth factor (TGF) α in both HCC cells and human squamous cell carcinoma cells undergoing apoptosis [6,7]. ACR induces the expression of interferon receptor, and also the expression and activity of signal transducer and activator of transcription (STAT) 1 during suppression of cell growth and induction of HCC cell apoptosis [8]. However, it is unclear whether these phenomena are dependent on the restoration of RARα/RXRα.

Transglutaminase 2 (TG2) is a member of a family of crosslinking enzymes that catalyze a post-translational modification of proteins by a calcium-dependent crosslinking reaction that forms N-ε (γ-glutamyl) lysine bonds [9-12]. TG2 has been implicated in apoptosis, although the mechanisms are unknown. Recently, we demonstrated that TG2 induces caspase-independent apoptosis in ethanol-treated hepatocytes by crosslinking and inactivation of the general transcription factor, Sp1, thereby reducing Sp1-dependent expression of growth factor receptors [9,13]. However, whether TG2-induced apoptosis pathway is involved in apoptotic signaling in other cell types or is induced by stimulation with anticancer reagents remains unclear.

Piedrafita *et al.* [14] reported that retinoid-induced apoptosis of T cells accompanies degradation of Sp1 downstream of the caspase pathway. Shao *et al.* [15] found that ACR inhibits the growth of HCC cells by reducing the expression of an Sp1-transactiviable gene, fibroblast growth factor receptor 3 (FGFR3) [16].

These reports suggest that Sp1 and/or its regulating genes are important in ACR-induced apoptosis pathway in HCC cells. We have therefore tested the hypothesis that ACR can restore the expression of TG2 by preventing phospho-inactivation of RXRα, and downregulate the expression of growth factor receptors by inactivating Sp1 due to both caspase-dependent degradation and TG2-dependent crosslinking. We have used HCC cells in culture and *in vivo* models of both transplantation of HCC into nude mice and *N*-diethylnitrosamine (DEN)-induced rat hepatocarcinogenesis.

Methods

Materials

ACR (NIK-333) was supplied from Kowa Company, Ltd. (Tokyo, Japan). Anti-TG2 monoclonal antibody (TGase II, Ab-1) was purchased from NeoMarkers (Fremont, CA). Anti-TG2 polyclonal antibody was produced as previously described [13]. Mouse anti-Sp1 (IC6), rabbit anti-Sp1 (PEP2), anti-EGFR, anti-c-Met, anti-FGFR1 antibodies were bought from Santa Cruz Biotechnology (Santa Cruz, CA).

Mouse anti-GAPDH antibody was from Millipore (Billerica, MA). Anti-Bcl-X_L and anti-cleaved caspase 3 antibodies were from Cell Signaling Technology (Danvers, MA). Horseradish peroxidase (HRP)-conjugated goat anti-rabbit or mouse IgG was from Jackson ImmunoResearch Laboratories (West Grove, PA). Viable cells were measured using a cell counting kit-8 (Dojindo; Tokyo, Japan). 5-(biotinamido) pentylamine, a biotinylated primary amine substrate for TG2 was provided by Pierce Biotechnology (Rockford, IL). A caspase-3 specific inhibitor, zDEVD-fmk, and Hoechst 33258 came from Calbiochem-Novabiochem (La Jolla, CA). Anti-crosslinked Sp1 (CLSp1) antibody was made in rabbits, and purified as previously described [13].

Cells and plasmids

A HCC cell line, JHH-7 cells kindly supplied by Dr. Matsuura (Jikei University School of Medicine, Tokyo, Japan) [17] were maintained in ASF104 medium (Ajinomoto, Tokyo, Japan). HC cells, a normal human hepatocyte cell line purchased from Cell Systems (Kirkland, WA), were cultured in CS-C complete medium (Kirkland, WA) [4]. HuH-7, HepG2, and HelaS3 cells were maintained in RPMI 1640 medium containing 10% FBS. The expression vector for human Sp1 (*Sp1-pCIneo*) was constructed as previously described [18]. The TG2, Sp1, and EGFR siRNA-expressing lentiviral vectors were constructed in the pSIH-H1 shRNA vector (SBI System Biosciences, CA). A GC3-Luc vector, containing 3 sequential repeats of GC box motifs derived from the *EGFR* promoter [19] and its TATA box sequence upstream of the luciferase cDNA, was generated by inserting a synthesized oligodeoxynucleotide cassette into the pGL3 vector (Promega Corp., WI).

Transient transfection

Transfections and assays of luciferase activity were performed with a combination of UNIFECTOR lipofection reagent (B-Bridge International, Inc.; Mountain View, CA) and luciferase reporter genes (firefly- and *Renilla*-Luc) as previously described [20], with further details being provided in the Additional file 1.

TG2 knockdown

Knockdown of TG2 was performed by transfection of anti-sense (AS) or siRNA to TG2 in JHH-7 cells, suppressing the expression of TG2 protein ~50% and ~70%, respectively (Additional file 2 Figure S1)

Preparation of whole lysates and nuclear extracts

Whole lysates were prepared in Hepes buffer containing 10 mM CHAPS and protease inhibitors. Nuclear extracts were prepared as previously described [20].

Western blotting

Western blotting was carried out as previously described [20], using combinations of 1 μg/ml each of anti-Sp1, anti-CLSp1, or anti-TG2 antibody and HRP-conjugated goat anti-rabbit/mouse IgG (1:1,000 dilution). Reactants were detected with Enhanced Chemiluminescence reagents (GE Healthcare, Buckinghamshire, UK).

Reverse transcriptase-polymerase chain reaction (RT-PCR)

RT-PCR was done as before [18], using sets of specific primers summarized in Additional file 3 Table S1.

Staining of cells

Cells grown on cover slips were fixed with 10% formalin in culture medium. They were permeabilized with 0.3% Triton X-100 in TBS (pH 7.4), and stained with the antibodies given in each figure legend. Apoptosis was detected by the terminal deoxynucleotidyl transferase-mediated dUTP nick end-labeling (TUNEL) method with the *In Situ* Cell Death Detection Kit (Roche Diagnostics GmbH; Mannheim, Germany). Digital images of cells were obtained by confocal microscope (Carl Zeiss, Inc. Germany), and digital images recorded.

Animal experiments

One week after JHH-7 cells (2×10^6 /50 μl) had been transplanted into the spleens of nude mice aged 6 weeks (Balb/c Slc-nu/nu, Japan SLC Inc., Shizuoka, Japan), ACR (100 mg/kg/day) or vehicle (soybean oil) was administrated by gavage at 10 μl/g body weight once a day on consecutive days for 3 weeks. The DEN-induced rat hepatocarcinogenesis model was used as previously described [21]. Briefly, 6-week old rats (F344/N SLC; Japan SLC Inc., Shizuoka, Japan) were given drinking water containing 40 ppm DEN (Tokyo Kasei Kogyo Co., Tokyo, Japan) for 15 weeks to produce liver neoplasms. ACR (40 and 80 mg/kg) or vehicle (soybean oil) was administered orally with a stomach tube at 5 μl/g body weight for 14 weeks. Experiments were performed in accordance with protocols approved by the RIKEN Institutional Animal Use and the Care Administrative Advisory Committees.

Immunohistochemistry

Immunohistochemistry were performed as before [13]. Livers were removed, fixed in 10% formalin, and embedded in paraffin wax. Sections were prepared and stained with anti-CLSp1, anti-TG2, anti-cleaved caspase 3, and anti-EGFR polyclonal antibodies. Staining signals were enhanced using an ABC kit (VECTASTAIN) and developed with DAB substrate.

Statistical analysis

Quantitative data are given as means ± SD. Student's *t* test was used to evaluate differences between 2 groups. In comparing data from the vehicle group with those from groups treated with ACR at doses of 25, 50, and 100 mg/kg body weight, the level of serum AFP and the number of AFP-positive mice were analyzed by Dunnett's multiple comparison and Fisher's exact probability test, respectively. A p-value of <0.05 was considered statistically significant.

Results

ACR induces both caspase- and TG2-dependent apoptosis pathways

ACR induced TUNEL-positive apoptosis of JHH-7 cells, but not normal hepatocyte HC cells (Figure 1A, *left panel*). Apoptotic JHH-7 cells were also positive for crosslinked Sp1 (CLSp1; Figure 1A, *right panel*). Strong immunofluorescent spots were obvious in cells undergoing severe apoptosis (Figure 1A, *right panel*, arrows). JHH-7 cells were the most sensitive to ACR of the 3 HCC cell lines (JHH-7, HuH-7, HepG2) and HelaS3 cells (Figure 1B). They showed similar TG2/TUNEL/CLSp1-positive apoptosis following ACR treatment (*data not shown*). Consistent with previous findings with another HCC cell line (HuH-7) [6], ACR treatment of JHH-7 cells, but not HC cells, suppressed phosphorylation of RXRα without affecting the expression of RXRα (Additional file 4 Figure S2A), prevented phospho-inactivation of RXRα, and enhanced the expression of TG2 (Additional file 4 Figure S2B).

Reciprocally in parallel with a dose- and time-dependent decrease in cell number (Figure 1C, *left panels*), both TUNEL (Figure 1C, *middle panels*) and TG2 positivity (Figure 1C, *right panels*) increased in ACR-treated JHH-7 cells undergoing apoptosis. ACR-induced apoptosis was partially blocked by either the inclusion of the caspase inhibitor, z-DEVD (Figure 1D and 1E, *sample 3*) or knocking down by 50% TG2 expression with antisense (AS) TG2 (Figure 1D and 1E, *sample 4*; Additional file 2 Figure S1A), whereas apoptosis was almost completely blocked by their combined inhibition (Figure 1D and 1E, *sample 5*). These results suggest that ACR-induced apoptosis is dependent on both caspase 3 and TG2 activation.

In ACR-treated JHH-7 cells ACR had markedly increased levels of CLSp1 (Figure 1A, *right panel* and Additional file 5 Figure S3A, *lane 4*), whereas levels of the Sp1 monomer decreased (Additional file 5 Figure S3A, *lane 2*), thereby reducing its DNA binding activity (Additional file 5 Figure S3B) and transactivation activity (Additional file 5 Figure S3C), as previously seen in ethanol-induced hepatocyte apoptosis [13]. Impaired Sp1 activity was partially improved either by inhibition of caspase or TG2 knockdown by transfection of ASTG, and almost completely restored by their combination, as also by overexpression of Sp1. These results suggest that

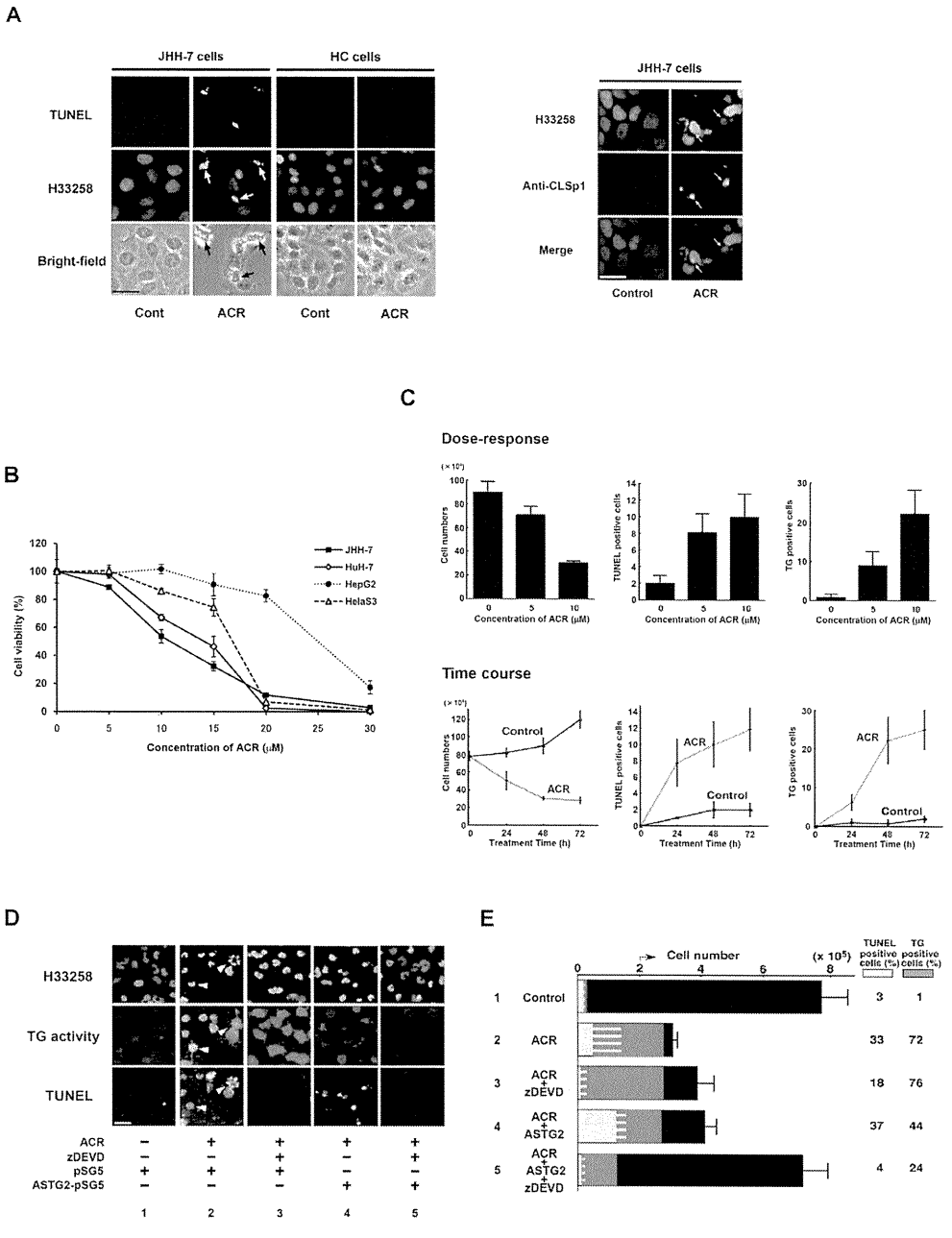

Figure 1 Induction of caspase 3 and TG2- dependent apoptosis by ACR in JHH-7 cell cultures. *A*, JHH-7 and HC cells were seeded in 35 mm dishes containing glass coverslips at 2 × 10^5/dish, and treated with 10 μM ACR or vehicle (0.1% ethanol) for 24 h. Cells were fixed and stained combination with Hoechst 33258, and TUNEL (*left panels*) or anti-CLSp1 antibody (*right panel*). Scale bar, 50 μm. *B*, JHH-7, HuH-7, HepG2 and HelaS3 were seeded at 1 × 10^4 cells/96 well microplates and treated with the indicated concentrations of ACR or vehicle for 24 h. Viable cell counts are plotted as percentages of each control culture treated with vehicle. *C*, JHH-7 cells were seeded as before and treated either with the indicated concentrations of ACR for 48 h, or with 10 μM ACR for the indicated times. Cells were fixed and stained with Hoechst 33258, TUNEL, and anti-TG2 antibody. The numbers of total and apoptotic cells with TUNEL or TG2 positivity in each dish were counted and plotted. *D*, JHH-7 cells were seeded as before and transfected with either pSG5 or anti-sense (AS) TG2-pSG5. The next day cells were treated with either vehicle or 10 μM ACR for 24 h in the presence or absence of 100 μM zDEVD-fmk, with 1 mM 5-(biotinamido)-pentylamine being included during the last 2 h incubation. Cells were fixed and stained with Hoechst 33258 (*upper panels*), TRITC-conjugated streptavidin (*middle panels*), and TUNEL (*bottom panels*). Arrowheads indicate apoptotic cells with chromatin condensation. Scale bar, 50 μm. *E*, JHH-7 cells were treated as in (*C*). The numbers of total and apoptotic cells with TUNEL (green colors) or TG2 (orange colors) positivity in each dish were counted and plotted as bar graphs. Their percentages relative to total cell number are given on the right hand-side of each bar graph. Panels *A-E* show representative results from 3 different experiments with similar results.

both caspase- and TG2-dependent pathways lead to silencing of Sp1 activity, which correlates with cell viability (Additional file 5 Figure S3D).

Reduced expression of growth factor receptors as the major Sp1 transcriptional targets in ACR-treated JHH-7 cells undergoing apoptosis

ACR-treated JHH-7 cells expressed decreased levels of EGFR at both mRNA (Figure 2A; 2.5-fold reduction in quantitative PCR) and protein (Figure 2B) levels. Although protein levels of c-Met and FGFR1 remained largely unaltered, mRNA levels of c-Met and FGFR1 decreased slightly following ACR-treatment. mRNA of Bcl-X_L was unchanged, but moderately altered at the protein level. ACR induced activation of caspase 3, but not its expression (Additional file 6 Figure S4A and S4B, *respectively*). While a single treatment with either a caspase inhibitor, z-DEVD (Figure 2C, *lane 4*) or overloading EGF (Figure 2C, *lane 6*) partially prevented a reduction in cell number in ACR-treated JHH-7 cells, combined treatment completely prevented this reduction (Figure 2C, *lane 8*).

To determine whether reduced expression of EGFR was due to Sp1 inactivation, transactivation of a chimeric reporter gene-construct in which expression was driven by 3 tandem functional GC box motifs derived from the EGFR promoter was monitored. ACR-treatment decreased the transactivational activity of the EGFR gene promoter (compare Figure 2D, *lanes 1 and 2*), which was partially prevented by overexpressing Sp1 (compare Figure 2D, *lanes 2 and 4*) or downregulating TG2 expression by 70% (compare Figure 2D, *lanes 2 and 6*; Additional file 2 Figure S1B). It was partially reversed by overexpression of TG2 (compare Figure 2D, *lanes 2 and 8*) and Sp1 inactivation with siRNA (compare Figure 2D, *lanes 2 and 10*). Sp1 inactivation with siRNA also reduced expression of EGFR protein (Figure 3A). In hepatocytes, treatment with Sp1 siRNA had previously decreased cell viability ([13]; *data not shown here*). siRNA knockdown of EGFR led to apoptosis (Figure 3B-3D). These results suggest that transcriptional reduction of *EGFR* due to a reduction in Sp1 activity may partially explain ACR-induced apoptosis of HCC cells.

ACR suppresses both transplant of human HCC cells in nude mice and DEN-induced rat hepatocarcinogenesis by inducing apoptosis accompanying the emergence of nuclear TG2 and CLSp1

Finally, the *in vivo* effect of ACR was examined in the 2 animal models. Using the transplant model in mice, where ACR dose-dependent reduction of serum levels of a tumor marker for HCC, α-fetoprotein (AFP) and the incidence of HCC (Additional file 7 Table S2), nuclear

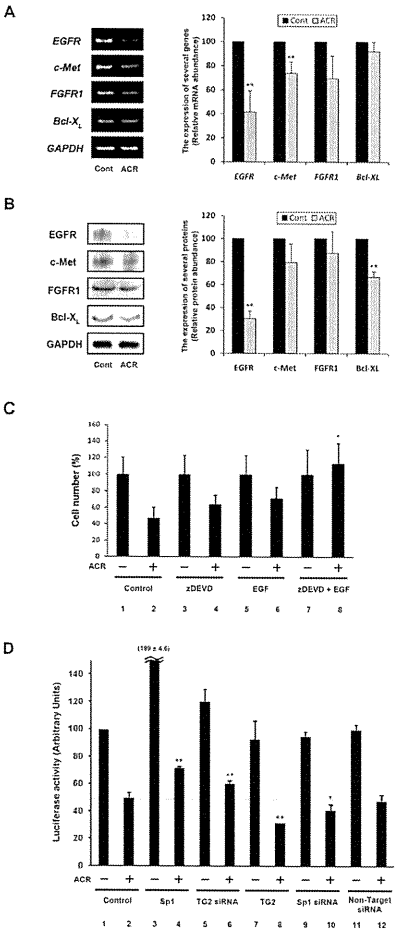

Figure 2 Induction of caspase 3- and TG2-dependent apoptosis by ACR via a reduction in the expression of EGFR due to silencing of Sp1. *A*, JHH-7 cells were treated with 10 μM ACR or vehicle for 12 h. Cells were harvested and mRNA expression of indicated genes was determined by RT-PCR. Bar graphs show densitometrically determined relative mRNA abundance normalized to *GAPDH* mRNA levels. **P < 0.01 compared to each control. *B*, JHH-7 cells were treated with 10 μM ACR or vehicle for 24 h. Cells were harvested and protein expression of indicated proteins was determined by Western blotting. The bar graph shows densitometrically determined relative protein abundance normalized to GAPDH protein levels. **P < 0.01 compared to each control. *C*, JHH-7 cells were treated with 10 μM ACR for 24 h in the presence or absence of 100 μM zDEVD, 50 ng/ml EGF or a combination of the two, and the numbers of viable cells were determined after trypsinization by Trypan Blue exclusion. Results shown are means ± SD (n = 3). *P < 0.05, compared to ACR-treated sample from control cells (*lane 2*). *D*, One day after transfection of JHH-7 cells with *EGFR* promoter GC3-Luc (1 μg/dish), cells were treated with 10 μM ACR for 24 h, co-transfected with Sp1 (*lanes 3 and 4*), TG2 shRNA (*lanes 5 and 6*), TG2 (*lanes 7 and 8*), Sp1 shRNA (*lanes 9 and 10*), and non-target siRNA (*lanes 11 and 12*) expression vector, and cell lysates were prepared. Luciferase activity of each cell lysate was determined. Results shown are means ± SD (n = 3). *P < 0.05, **P < 0.01 compared to ACR-treated control sample from control cells (*lane 2*). *Panels A-D* show representative results from three different experiments with similar results.

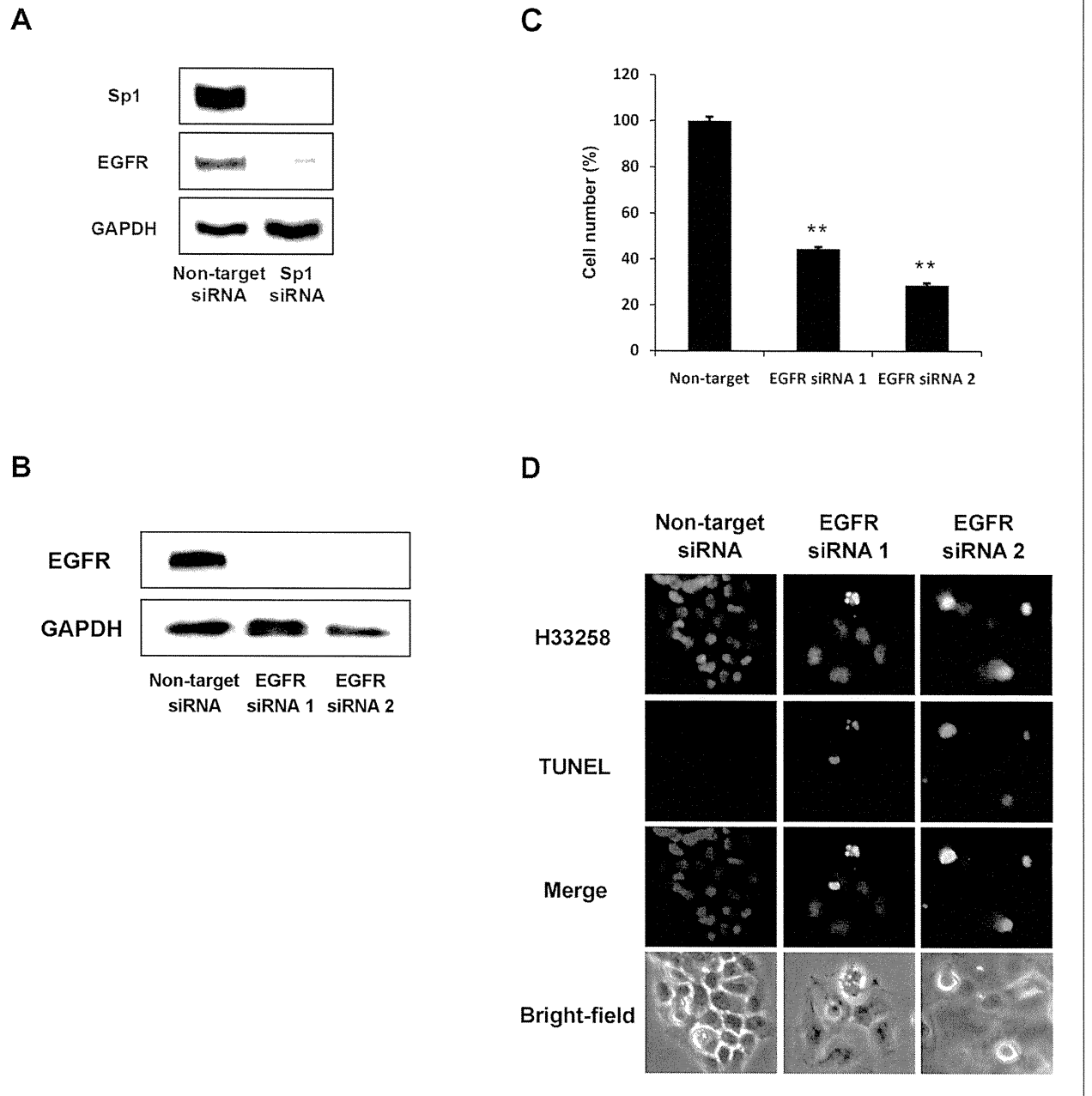

Figure 3 Induction of apoptosis in JHH-7 cells using Sp1 and EGFR siRNAs. *A*, JHH-7 cells overexpressing non-target or Sp1 siRNA were harvested and protein levels of Sp1, EGFR, and GAPDH determined by Western blotting. *B*, JHH-7 cells overexpressing non-target or 2 kinds of EGFR siRNAs were harvested and protein levels of EGFR and GAPDH determined by Western blotting. *C*, Numbers of viable cells were counted 2 days after seeding these cells on 35 mm dishes. Results shown are the number of viable cells relative to the controls, expressed as % ± S.D. **P < 0.01 compared to control cells. *D*, The seeded cells on cover slips in 35 mm dishes were fixed and stained with Hoechst (*upper panels*) and TUNEL (*second panels*). *Panels A-D* show representative results from 3 different experiments with similar results.

TG2 and CLSp1 increased in cancerous liver cells of ACR-treated nude mice transplanted with the JHH-7 cell line (Figure 4A, *panels A and B, respectively*) compared with adjacent normal liver (Figure 4A, *panels D and E*). Significant induction of TG2 and activation of caspase 3 occurred in metastatic areas in nude mice transplanted with JHH-7 cells after treatment with ACR (Figure 4A, *panels A and C, respectively*). Moreover, EGFR levels in the metastatic areas were lower than in normal areas of the same liver (compare Figure 4A, *panels G and J*). Similar results were obtained in the rat model of DEN-induced hepatocarcinogenesis, in which

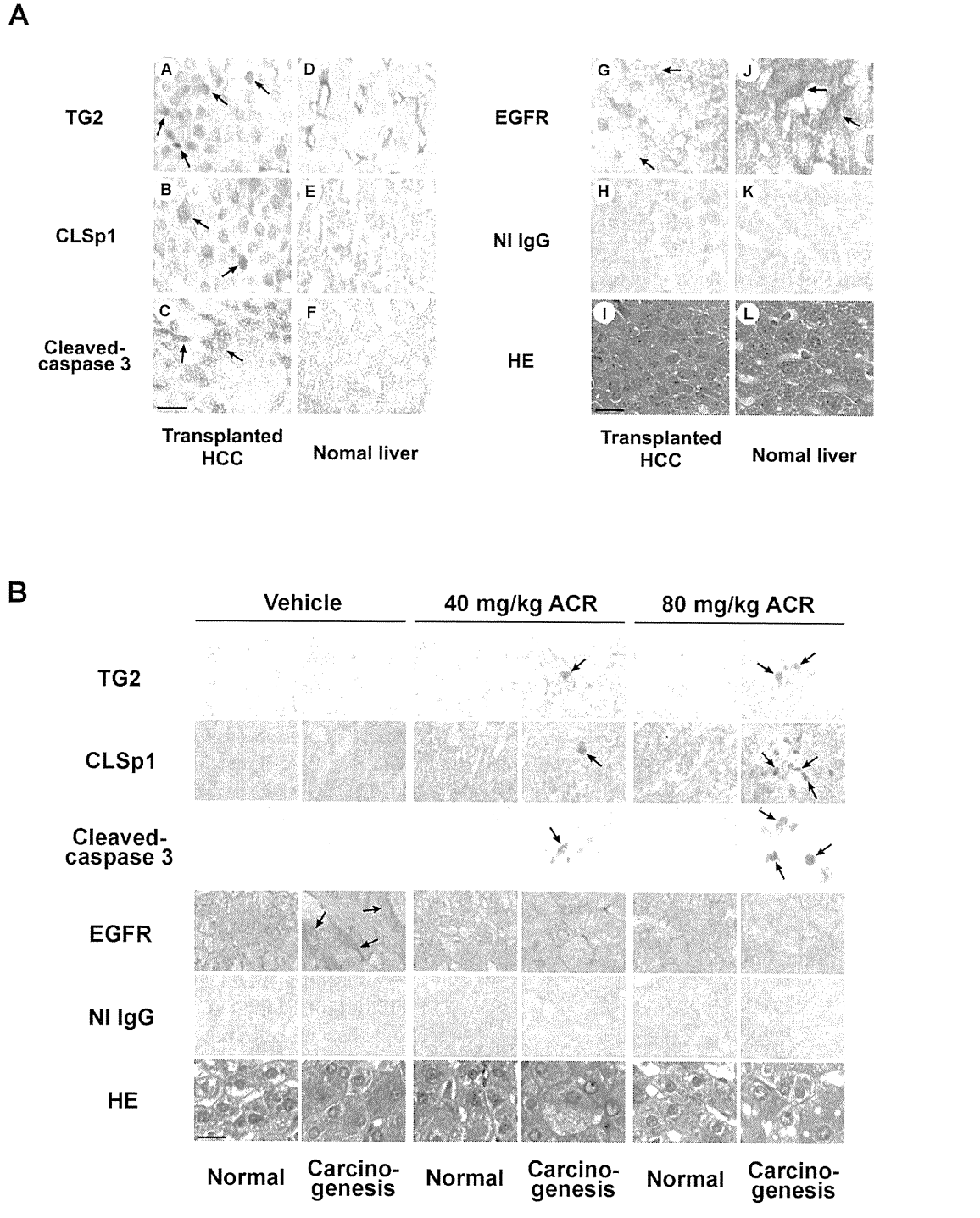

Figure 4 Nuclear accumulation of TG2 and CLSp1 observed in the liver of nude mice transplanted with JHH-7 cells, and in DEN-treated rats with liver cancer after ACR treatment. *A*, Liver sections including normal (*panels D-F and J-L*) and metastatic areas (*panels A-C and G-I*) from JHH-transplanted nude mice following treatment with ACR were stained with polyclonal anti-TG2 (30 μg/ml; *panels A, D*), anti-CLSp1 (30 μg/ml; *panels B, E*), anti-cleaved caspase 3 (10 μg/ml; *panels C, F*), anti-EGFR (10 μg/ml; *panels G, J*), and non-immune antibodies (NI IgG; 30 μg/ml; *panels H, K*). *B*, Liver sections from normal and neoplastic areas in DEN-treated rats following treatment with vehicle or ACR (at 40 and 80 mg/kg) were stained as in Figure 4A. The signals were enhanced with an ABC kit and developed with DAB substrate. Sections were counterstained with hematoxylin-eosin (HE; Figure 4A, *panels I, L*, and Figure 4B, *bottom panels*). Arrows indicate signals under the levels for each antigen. Scale bar, 50 μm.

ACR's anti-cancer effect has been reported [21]. Simultaneous induction of TG2, CLSp1, and activation of caspase 3 occurred in paralleled with a reduction in EGFR (Figure 4B).

Discussion

The data show that: (i) ACR suppresses the hyper-phosphorylation of RXRα, restored its transcriptional function, and enhanced the expression of TG2 and its nuclear accumulation, along with caspase 3 activation; (ii) Sp1 is crosslinked by TG2 and degraded by caspase 3, resulting in loss of its activity; and (iii) expression of Sp1-regulated target genes, such as EGFR (critical for cell survival), decrease, culminating in apoptosis of the cancer cells (Figure 5). The results of *in vitro* findings were confirmed by the *in vivo* models of nude mice transplanted with JHH-7 cells and DEN-induced hepatocarcinogenesis in rats (Figure 4). The recurrence of HCC in these animal models remains to be elucidated.

ACR treatment induced apoptosis in HCC cells (JHH-7 and HuH-7), but not in normal hepatocyte cells (HC cells) (Figure 1A and 1B). As a clue to a reason for the difference, we found that both expression and phosphorylation levels of RXRα were much higher in HCC cells than in HC cells, and that ACR suppressed its phosphorylation levels without altering its expression level (Additional file 4 Figure S2A), as previously shown [5]. In further previous work, we had demonstrated that 2 amino acids in RXRα, T82 and S260, were phosphorylated in HCC, but not in HC cells [4]. Therefore, phosphorylation of RXRα observed in JHH-7 cells was referred to as "hyperphosphorylation". However, RARα and RARβ were phosphorylated not only in JHH-7 cells, but also in HC cells, and ACR downregulated their phosphorylation in both cases (Additional file 4 Figure S2A). Phosphorylation was not detected in the other 3 subtypes of RXR and RAR (Additional file 4 Figure S2A). Therefore, phosphorylation of RXRα was only specific in cancer cells, which could be a reason for the selective apoptosis of cancer cells by ACR treatment.

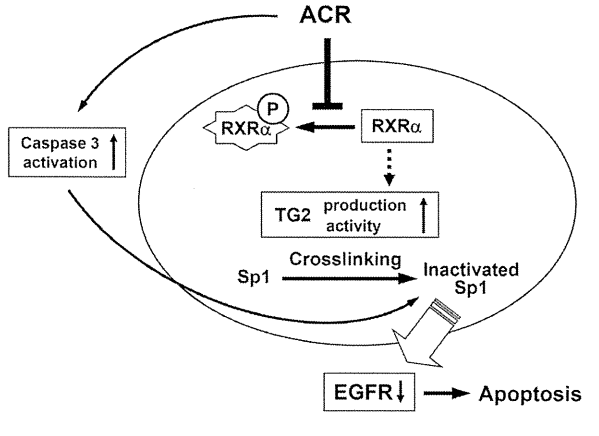

Figure 5 Schematic diagram showing the molecular mechanism by which ACR causes HCC apoptosis by restorating phospho-inactivated RXRα followed by enhanced TG2-mediated crosslinking/silencing of Sp1, thereby reducing EGFR-medicated EGF signaling.

It is noteworthy that treatment with either antisense of TG2 or inhibitors of caspase 3 only partially blocked ACR-induced apoptosis, whereas their simultaneous inhibition completely prevented apoptosis, suggesting that TG2 and caspase 3 contribute independently to the induction of apoptosis (Figure 1D and 1E). We measured the activity of caspase 3 and TG2 in the presence of an inhibitor of each other's enzyme, such as zDEVD and cystamine. When cystamine suppressed ~50% of ACR induction in TG2 activity (compare the differences between *lanes 1 and 4* with those between *lanes 2 and 5* in Additional file 6 Figure S4D), it suppressed 60% of ACR induction in caspase 3 activity (compare the differences between *lanes 1 and 4* with those between *lanes 2 and 5* in Additional file 6 Figure S4C). On the other hand, when zDEVD completely suppressed ACR-induced increase in caspase 3 activity (compare the differences between *lanes 1 and 4* with those between *lanes 3 and 6* in Additional file 6 Figure S4C), 50% of an increase in the TG2 activity remained (compare the differences with *lanes 1 and 4* with those between *lanes 3 and 6* in Additional file 6 Figure S4D). The data suggest that TG2 and caspase 3 influenced each other with a higher hierarchy of TG2 over caspase 3 in the contribution to the apoptosis of HCC induced by ACR. Synergism between inhibition in caspase and overloading of EGF in preventing apoptosis also suggests that both the caspase 3- and EGFR-dependent pathways exist (Figure 2C).

Expression of EGFR is regulated by Sp1 [19,22], and inhibition of EGFR signaling leads to growth inhibition, apoptosis, and cell cycle arrest of HCC cells [23,24]. We have linked these findings by showing that the downregulation of EGFR with siRNA induces apoptosis (Figure 3B-D), suggesting that inhibiting EGFR signaling via silencing Sp1 is a promising treatment strategy against HCC.

Induction of CLSp1 and the subsequent reduction in EGFR has been reproduced in ACR-treated HuH-7 cells (*data not shown*). In contrast, although Shao *et al.* [15] reported that ACR inhibits the cell growth through downregulation of FGFR3 expression and FGF-mediated signaling in HepG2 cells, this was not found to be the case in our ACR-treated JHH-7 cells (*data not shown*). These findings suggest that HCC cell lines differ in the way that growth factor receptors are involved in survival.

Whereas TG2 may be a substrate of caspase 3 during apoptosis of thymocytes, resulting in loss of transamidating function [25], TG2 in turn inhibits of apoptosis due to crosslinking and inactivation of caspase 3 in thapsigargin-mediated apoptosis of colon carcinoma cells [26]. In the latter article, thapsigargin treatment generated 2 additional biologically inactive species of caspase 3, viz. p40 and p64, via TG2-mediated crosslinking of caspase 3, thereby protecting cells from apoptosis. However, we failed to detect either p40 or p64 in our ACR-treated JHH-7 cells. We speculate that crosslinking of caspase 3 would be induced specifically by treatment with thapsigargin. Our data clearly shows that both caspase 3 and TG2 are functional in ACR-treated HCC cells, without apparent alteration of caspase 3 expression (Additional file 6 Figure S4A and 4B). These controversial results might be ascribed to differences in cell types and the nature of the apoptotic stimuli, although the precise mechanisms need to be elucidated.

Piedrafita and Pfahl [14] reported that caspase 3 directly cleaved and inactivated Sp1 in retinoid-treated T cells undergoing apoptosis. They showed that cleavages of PARP and Sp1 were simultaneously induced by caspase 3 and prevented with caspase inhibitors (zVAD-fmk and zDEVD-fmk). We anticipated that CLSp1 might also be partially cleaved by caspase 3; however, as molecular size differences would be too small to be recognized on the gel against a high molecular weight of CLSp1 detected at the top of the gel, we found no band shifts due to the cleavage. Hence, the possibility of simultaneous crosslinking and cleavage of Sp1 by TG2 and caspase 3, respectively, cannot be ruled out, even though we saw no truncated Sp1 with a Mw of 68 kD in ACR-treated HCC cells.

ACR-treated JHH show enhanced nuclear localization of TG2; nuclear localization of TG2 is also important for induction of TG2-dependent apoptosis. Peng *et al.* [27] reported that TG2 binds importin-α3, an important factor in nuclear translocation, and therefore we are investigating the detail mechanism of TG2 nuclear localization accompanying ACR-induced apoptosis.

Conclusions

Our new findings indicate that ACR induces both activation of caspase 3 as well as the expression and activation of TG2, which together initiate the apoptotic pathway via degrading/crosslinking and inactivation of the transcription factor, Sp1. Reduced expression of growth factor receptor genes (*e.g.* EGFR) also occurs. This dual activation of both caspase and TG-dependent apoptotic pathways could in part be central as mechanisms by which ACR inhibits tumor cell growth, resulting in the prevention of secondary tumors after treatment of primary HCCs (Figure 5). Future study should establish the possibility that regulation of TG2-dependent apoptotic pathway may help in the development of new therapies for the prevention of HCC.

Additional material

Additional file 1: Additional text. This text contains the additional "Methods" and "References"

Additional file 2: Figure S1: Efficiency of transfection with anti-sense and siRNA to TG2 in JHH-7 cells. *A*, JHH-7 cells were seeded in 60 mm dishes at 6 × 10^5/dish, and transfected with 4 μg of either empty vector (pSG5) or ASTG2-pSG5. Cells were harvested and the expression level of TG2 determined by Western blotting. Upper numbers in parentheses show the densitometrically determined relative protein abundance. *B*, JHH-7 cells were seeded in 60 mm dishes at 6 × 10^5/dish, and transfected with 4 μg of vectors expressing either non-target siRNA or TG2 siRNA. Cells were harvested and the expression level of TG2 determined by Western blotting. Upper numbers in parentheses show the densitometrically determined relative protein abundance. *Panels A and B* show representative results from 3 different experiments with similar results.

Additional file 3: Table S1: Primers for RT-PCR and quantitative-PCR experiments. The list of used specific primers for RT-PCR.

Additional file 4: Figure S2: ACR prevented phosphorylation and inactivation of RXRα, and stimulated the expression of TG2 in JHH-7 cells. *A*, JHH-7 cells (*lane 1 and 2*) and HC cells (*lane 3 and 4*) were treated with 10 μM ACR or vehicle for 12 h. Cells were harvested and nuclear extracts were prepared. Phosphoproteins affinity-purified from each nuclear extract using the Phosphoprotein Purification Kit (QIAGEN) (*left panel*) as well as whole nuclear extracts (*right panel*), were subjected to SDS-PAGE, followed by Western blotting using the indicated antibodies against 6 different RXR/RAR or GAPDH. *B*, JHH-7 cells were transfected with either an empty vector (*columns 1-4*) or vectors expressing wild-type RXRα (*columns 5-8*), its alanine mutant T82A (unphosphorylated form; *columns 9-12*), or its aspartate mutant T82 D (phosphomimic; *columns 13-16*). The next day cells were treated either with 9-*cis* RA (9cRA; 6 μM) or its vehicle, or with and/or ACR (10 μM) for 24 h. Subsequently, levels of *TG2* mRNA in cell lysates were quantified by RT-PCR (*upper panels*) and quantitative-PCR (*lower graphs*), where relative expression levels of TG2 were calculated in comparison with each control and then plotted. Treatment with 1 μM 9-cis-RA also gave basically similar results (data not shown), but the data obtained under treatment with 6 μM 9-cis-RA are shown here, giving the more significant differences. *Panels A and B* show representative results from 3 different experiments with similar results.

Additional file 5: Figure S3: Crosslinking and silencing of Sp1 in ACR-treated JHH-7 cell cultures undergoing apoptosis and its reversion by overexpression of Sp1. *A*, JHH-7 cells were treated with 10 μM ACR for 24 h. The cells were harvested and nuclear extracts prepared. The levels of Sp1 and CLSp1 were assessed by Western blotting with an anti-Sp1 (*columns 1 and 2*) and CLSp1 (*columns 3 and 4*) antibodies, respectively. *B*, JHH-7 cells were transfected with 1.5 μg of either combination of *pCIneo*, *pSG5*, *Sp1-pCIneo*, or *anti-sense (AS) TG2-pSG5*. The next day they were treated with either 10 μM ACR or its vehicle in the presence or absence of 100 μM zDEVD-fmk for 24 h. Cells were harvested and nuclear extracts prepared. Sp1 DNA-binding activity of each nuclear extract (10 μg protein) was determined by gel-shift assay, using a consensus GC box as a probe (+cold; nuclear extracts + 50-fold excess of unlabeled probe, +anti-Sp1 IgG; nuclear extracts + 2 μg of anti-Sp1 antibody, +NI IgG; nuclear extracts + 2 μg of non-immune IgG). *C*, JHH-7 cells were transfected with 1.5 μg of a consensus GC3-Luc reporter and *Renilla*-Luc, plus a combination of *pCIneo*, *pSG5*, *Sp1-pCIneo* or *anti-sense (AS) TG2-pSG5*. The next day the cells were treated with 10 μM ACR for 24 h in the presence or absence of 100 μM zDEVD-fmk. Cell lysates were prepared and luciferase activity of each cell lysate determined. Results are means ± SD (n = 3). *D*, JHH-7 cells were

transfected with either a combination of *pCIneo, pSG5, anti-sense (AS) TG2-pSG5, Sp1-pCIneo, Sp1 C domain-pCIneo, ΔC Sp1-pCIneo*. The next day the cells were treated with 10 μM ACR for 24 h. The number of viable cells was determined. Results are means ± SD (n = 4). *Panels A-D* show representative results from 3 different experiments with similar results.

Additional file 6: Figure S4: ACR stimulated activation of caspase 3 and TG2 in JHH-7 cells and the crosstalk between these proteins. *A and B*, JHH-7 cells were treated with 10 μM ACR or the vehicle for 24 h. Cells were harvested and protein levels of activated caspase 3 and GAPDH determined by Western blots, using anti-cleaved-caspase 3 and anti-GAPDH antibodies (*A*); each of their mRNA expression was determined by RT-PCR (*B*). *C*, JHH-7 cells was seeded at 1×10^4 cells/96 well microplates and treated with 10 μM ACR or vehicle (0.1% ethanol) for 5 h in the presence or absence of either 100 μM zDEVD-fmk or 100 μM cystamine with 0.2 mM 5-(biotinamido)-pentylamine. Caspase 3 activity was measured using a Caspase-Glo 3/7 assay kit (Promega Corp., WI) as described in attached manual. Relative caspase 3 activity of each sample was calculated by normalization with the number of viable cells in the same sample measured with a cell counting kit-8 (Dojindo; Tokyo, Japan). *D*, JHH-7 cells seeded in 100 mm dishes at 1.6×10^6/dish were treated as in (C). TG2 activity was measured as described in Additional file 1. Relative TG2 activity of each sample was calculated by normalization with the number of viable cells in the same sample, measured with a cell counting kit-8 (Dojindo; Tokyo, Japan). *Panels A-D* show representative results from 3 different experiments with similar results.

Additional file 7: Table S2: Suppression by ACR of metastasis and growth of human HCC cell line, JHH-7 cells transplanted into nude mice. Nude mice that had been transplanted with JHH-7 were given orally with ACR with increasing concentrations (25, 50, and 100 mg/kg/day) as described detailed in the "Methods". Serum AFP was measured. Incidence was calculated based on level of the positive-AFP (more than 6 ng/ml). Cisplatin was used as a positive control. *p < 0.05 compared to control (Dunnett's multiple comparison test), #p < 0.05 compared to control (Fisher exact test)..

List of abbreviations

9-*cis* RA: 9-*cis* retinoic acid; ACR: acyclic retinoid; CLSp1: crosslinked Sp1; DEN: *N*-diethylnitrosamine; EGFR: epidermal growth factor receptor; FGFR3: fibroblast growth factor receptor 3; HCC: hepatocellular carcinoma; RXR: retinoid X receptor; TG2: transglutaminase 2.

Acknowledgements

We thank Dr. Matsushima-Nishiwaki (Gifu University, Gifu, Japan) for useful discussion. This work was supported partly by Grant-in-Aids from the Ministry of Education, Science, Sports and Culture (20390215, S.K.; 17015016, H.M.; 22790266, H.T.), a grant for the "Chemical Genomics Research Program" (to SK), and "Special Grant for Promotion of Research" (to HT) from RIKEN.

Author details

[1]Molecular Ligand Biology Research Team, Chemical Genomics Research Group, Chemical Biology Department, RIKEN Advanced Science Institute, Wako, Saitama 351-0198, Japan. [2]Pharmaceutical Development, Pharmaceutical Division, KOWA Company, Ltd., Chuo, Tokyo 103-8433, Japan. [3]Tokyo New Drug Research Laboratories, Pharmaceutical Division, KOWA Company, Ltd., Higashimurayama, Tokyo 189-0022, Japan. [4]Department of Gastroenterology, Gifu University School of Medicine, Gifu 501-1194, Japan.

Authors' contributions

HT and TS performed the research, analyzed the data, and drafted the manuscript. YF helped with cell culture, transfection, immunostaining and Western blotting techniques. NI prepared the acyclic retinoid used in these studies. MW helped with immunostaining techniques. MO, HM and SK designed the research, interpreted the data, and revised the manuscript. All authors approved the final version of the manuscript.

Competing interests

The authors declare that they have no competing interests.

Received: 5 June 2010 Accepted: 9 January 2011
Published: 9 January 2011

References

1. El-Serag HB: **Hepatocellular carcinoma and hepatitis C in the United States.** *Hepatology* 2002, **36**:S74-S83.
2. Muto Y, Moriwaki H, Ninomiya M, Adachi S, Saito A, Takasaki KT, Tanaka T, Tsurumi K, Okuno M, Tomita E, Nakamura T, Kojima T: **Prevention of second primary tumors by an acyclic retinoid, polyprenoic acid, in patients with hepatocellular carcinoma. Hepatoma Prevention Study Group.** *N Engl J Med* 1996, **334**:1561-1567.
3. Takai K, Okuno M, Yasuda I, Matsushima-Nishiwaki R, Uematsu T, Tsurumi H, Shiratori Y, Muto Y, Moriwaki H: **Prevention of second primary tumors by an acyclic retinoid in patients with hepatocellular carcinoma. Updated analysis of the long-term follow-up data.** *Intervirology* 2005, **48**:39-45.
4. Matsushima-Nishiwaki R, Okuno M, Adachi S, Sano T, Akita K, Moriwaki H, Friedman SL, Kojima S: **Phosphorylation of retinoid X receptor α at serine 260 impairs its metabolism and function in human hepatocellular carcinoma.** *Cancer Res* 2001, **61**:7675-7682.
5. Matsushima-Nishiwaki R, Okuno M, Takano Y, Kojima S, Friedman SL, Moriwaki H: **Molecular mechanism for growth suppression of human hepatocellular carcinoma cells by acyclic retinoid.** *Carcinogenesis* 2003, **24**:1353-1359.
6. Nakamura N, Shidoji Y, Moriwaki H, Muto Y: **Apoptosis in human hepatoma cell line induced by 4,5-didehydro geranylgeranoic acid (acyclic retinoid) via down-regulation of transforming growth factor-α.** *Biochem Biophys Res Commun* 1996, **219**:100-104.
7. Shimizu M, Suzui M, Deguchi A, Lim JT, Weinstein IB: **Effects of acyclic retinoid on growth, cell cycle control, epidermal growth factor receptor signaling, and gene expression in human squamous cell carcinoma cells.** *Clin Cancer Res* 2004, **10**:1130-1140.
8. Obora A, Shiratori Y, Okuno M, Adachi S, Takano Y, Matsushima-Nishiwaki R, Yasuda I, Yamada Y, Akita K, Sano T, Shimada J, Kojima S, Okano Y, Friedman SL, Moriwaki H: **Synergistic induction of apoptosis by acyclic retinoid and interferon-beta in human hepatocellular carcinoma cells.** *Hepatology* 2002, **36**:1115-1124.
9. Iismaa SE, Mearns BM, Lorand L, Graham RM: **Transglutaminases and disease: lessons from genetically engineered mouse models and inherited disorders.** *Physiol Rev* 2009, **89**:991-1023.
10. Lorand L, Graham RM: **Transglutaminases: crosslinking enzymes with pleiotropic functions.** *Nat Rev Mol Cell Biol* 2003, **4**:140-156.
11. Fesus L, Piacentini M: **Transglutaminase 2: an enigmatic enzyme with diverse functions.** *Trends Biochem Sci* 2002, **27**:534-539.
12. Griffin M, Casadio R, Bergamini CM: **Transglutaminases: nature's biological glues.** *Biochem J* 2002, **368**:377-396.
13. Tatsukawa H, Fukaya Y, Frampton G, Martinez-Fuentes A, Suzuki K, Kuo TF, Nagatsuma K, Shimokado K, Okuno M, Wu J, Iismaa S, Matsuura T, Tsukamoto H, Zern MA, Graham RM, Kojima S: **Role of transglutaminase 2 in liver injury via cross-linking and silencing of transcription factor Sp1.** *Gastroenterology* 2009, **136**:1783-95.
14. Piedrafita FJ, Pfahl M: **Retinoid-induced apoptosis and Sp1 cleavage occur independently of transcription and require caspase activation.** *Mol Cell Biol* 1997, **17**:6348-6358.
15. Shao RX, Otsuka M, Kato N, Taniguchi H, Hoshida Y, Moriyama M, Kawabe T, Omata M: **Acyclic retinoid inhibits human hepatoma cell growth by suppressing fibroblast growth factor-mediated signaling pathways.** *Gastroenterology* 2005, **128**:86-95.
16. McEwen DG, Ornitz DM: **Regulation of the fibroblast growth factor receptor 3 promoter and intron I enhancer by Sp1 family transcription factors.** *J Biol Chem* 1998, **273**:5349-5357.
17. Fujise K, Nagamori S, Hasumura S, Homma S, Sujino H, Matsuura T, Shimizu K, Niiya M, Kameda H, Fujita K: **Integration of hepatitis B virus DNA into cells of six established human hepatocellular carcinoma cell lines.** *Hepatogastroenterology* 1990, **37**:457-460.
18. Botella LM, Sanchez-Elsner T, Sanz-Rodriguez F, Kojima S, Shimada J, Guerrero-Esteo M, Cooreman MP, Ratziu V, Langa C, Vary CP, Ramirez JR, Friedman S, Bernabeu C: **Transcriptional activation of endoglin and transforming growth factor-β signaling components by cooperative interaction between Sp1 and KLF6: their potential role in the response to vascular injury.** *Blood* 2002, **100**:4001-4010.

19. Kageyama R, Merlino GT, Pastan I: **Epidermal growth factor (EGF) receptor gene transcription. Requirement for Sp1 and an EGF receptor-specific factor.** *J Biol Chem* 1988, **263**:6329-6336.
20. Shimada J, Suzuki Y, Kim SJ, Wang PC, Matsumura M, Kojima S: **Transactivation via RAR/RXR-Sp1 interaction: characterization of binding between Sp1 and GC box motif.** *Mol Endocrinol* 2001, **15**:1677-1692.
21. Kagawa M, Sano T, Ishibashi N, Hashimoto M, Okuno M, Moriwaki H, Suzuki R, Kohno H, Tanaka T: **An acyclic retinoid, NIK-333, inhibits N-diethylnitrosamine-induced rat hepatocarcinogenesis through suppression of TGF-α expression and cell proliferation.** *Carcinogenesis* 2004, **25**:979-985.
22. Kitadai Y, Yasui W, Yokozaki H, Kuniyasu H, Haruma K, Kajiyama G, Tahara E: **The level of a transcription factor Sp1 is correlated with the expression of EGF receptor in human gastric carcinomas.** *Biochem Biophys Res Commun* 1992, **189**:1342-1348.
23. Schiffer E, Housset C, Cacheux W, Wendum D, Desbois-Mouthon C, Rey C, Clergue F, Poupon R, Barbu V, Rosmorduc O: **Gefitinib, an EGFR inhibitor, prevents hepatocellular carcinoma development in the rat liver with cirrhosis.** *Hepatology* 2005, **41**:307-314.
24. Huether A, Hopfner M, Sutter AP, Schuppan D, Scherubl H: **Erlotinib induces cell cycle arrest and apoptosis in hepatocellular cancer cells and enhances chemosensitivity towards cytostatics.** *J Hepatol* 2005, **43**:661-669.
25. Fabbi M, Marimpietri D, Martini S, Brancolini C, Amoresano A, Scaloni A, Bargellesi A, Cosulich E: **Tissue transglutaminase is a caspase substrate during apoptosis. Cleavage causes loss of transamidating function and is a biochemical marker of caspase 3 activation.** *Cell Death Differ* 1999, **6**:992-1001.
26. Yamaguchi H, Wang HG: **Tissue transglutaminase serves as an inhibitor of apoptosis by cross-linking caspase 3 in thapsigargin-treated cells.** *Mol Cell Biol* 2006, **26**:569-579.
27. Peng X, Zhang Y, Zhang H, Graner S, Williams JF, Levitt ML, Lokshin A: **Interaction of tissue transglutaminase with nuclear transport protein importin-α3.** *FEBS Lett* 1999, **446**:35-39.

doi:10.1186/1476-4598-10-4
Cite this article as: Tatsukawa *et al.*: Dual induction of caspase 3- and transglutaminase-dependent apoptosis by acyclic retinoid in hepatocellular carcinoma cells. *Molecular Cancer* 2011 **10**:4.

Ability of IDO To Attenuate Liver Injury in α-Galactosylceramide–Induced Hepatitis Model

Hiroyasu Ito,* Masato Hoshi,* Hirofumi Ohtaki,* Ayako Taguchi,† Kazuki Ando,*,‡ Tetsuya Ishikawa,§ Yosuke Osawa,* Akira Hara,† Hisataka Moriwaki,¶ Kuniaki Saito,‖ and Mitsuru Seishima*

IDO converts tryptophan to L-kynurenine, and it is noted as a relevant molecule in promoting tolerance and suppressing adaptive immunity. In this study, we examined the effect of IDO in α-galactosylceramide (α-GalCer)–induced hepatitis. The increase in IDO expression in the liver of wild-type (WT) mice administered α-GalCer was confirmed by real-time PCR, Western blotting, and IDO immunohistochemical analysis. The serum alanine aminotransferase levels in IDO-knockout (KO) mice after α-GalCer injection significantly increased compared with those in WT mice. 1-Methyl-D-tryptophan also exacerbated liver injury in this murine hepatitis model. In α-GalCer–induced hepatitis models, TNF-α is critical in the development of liver injury. The mRNA expression and protein level of TNF-α in the liver from IDO-KO mice were more enhanced compared with those in WT mice. The phenotypes of intrahepatic lymphocytes from WT mice and IDO-KO mice treated with α-GalCer were analyzed by flow cytometry, and the numbers of $CD49b^+$ and $CD11b^+$ cells were found to have increased in IDO-KO mice. Moreover, as a result of the increase in the number of NK cells and macrophages in the liver of IDO-KO mice injected with α-GalCer, TNF-α secretion in these mice was greater than that in WT mice. Deficiency of IDO exacerbated liver injury in α-GalCer–induced hepatitis. IDO induced by proinflammatory cytokines may decrease the number of TNF-α–producing immune cells in the liver. Thus, IDO may suppress overactive immune response in the α-GalCer–induced hepatitis model. *The Journal of Immunology,* **2010, 185: 4554–4560.**

Indoleamine 2,3-dioxygenase has been identified as an enzyme that has powerful immunomodulatory effects, resulting from its enzymatic activity, which leads to catabolism of the essential amino acid L-tryptophan (L-Trp) to L-kynurenine (L-Kyn) (1, 2). This enzyme is expressed in epithelial, macrophage, and dendritic cells induced by proinflammatory cytokines, including type I and type II IFN (3, 4). The binding of CTLA-4 with CD80/CD86 on the membrane of dendritic cells also stimulates IDO transcriptional expression and activity (5, 6). Furthermore, metabolites of the L-Kyn pathway have been shown to act as immunoregulatory molecules that have immunosuppressive effects in the tissue microenvironment (7). IDO and the L-Trp pathway play critical roles in the generation of immune tolerance against foreign Ags in tissue microenvironments. Recently, we demonstrated that IDO expression on hepatocytes is increased in liver injury caused by hepatitis B virus-specific CTL in hepatitis B virus transgenic mice (8). Furthermore, it has been reported that IDO expressions in the liver and serum L-Kyn/L-Trp ratios in patients with chronic hepatitis C were increased and that this upregulation of IDO was caused by the IFN-γ produced by hepatitis C virus-activated T cells in the liver (9). As shown above, IDO expression is significantly enhanced during liver injury. We therefore established two hypotheses on the role of IDO: 1) IDO directly or indirectly brings about the progression of liver injury; and 2) IDO production is enhanced as a protective mechanism in liver injury. However, the actual role of IDO in liver injury remains unknown.

Several reports have demonstrated that α-galactosylceramide (α-GalCer), a specific ligand for invariant Vα14 NKT cells, induces liver injury (10–12). α-GalCer is hepatotoxic since the administration of α-GalCer in mice results in the activation and apoptosis of hepatic Vα14 NKT cells via activation-induced cell death and associated liver damage. Furthermore, the hepatotoxic effect of α-GalCer was found to be mediated by TNF-α produced by activated hepatic Vα14 NKT cells (12). In fact, it was proposed that TNF-α increases FasL expression on Vα14 NKT cells, and that these cells in turn promote liver damage by interacting with Fas-expressing hepatocytes (12). It is noteworthy that liver injury induced by α-GalCer is thought to potentially mimic some aspects of autoimmune hepatitis. The liver appears to be particularly susceptible to injury as a result of increased immune responses, mainly mediated by T lymphocytes and/or emerging autoantibodies. On viral infection of hepatocytes, the cytopathic effect of the virus per se is only moderate; instead, liver damage is caused by cellular immune responses to infected cells. Thus, the host immune system is related to the initiation and progression of liver injury in several liver injury models, and it is very important to determine the role of IDO and its powerful immunomodulatory effects during hepatic injury.

In this study, we examined the effect of IDO on α-GalCer–induced liver injury in mice and demonstrated that liver injury was exacerbated in IDO-deficient mice.

*Department of Informative Clinical Medicine, †Department of Tumor Pathology, and ¶First Department of Internal Medicine, Gifu University Graduate School of Medicine, Gifu; ‡Goto Clinic, Ogaki; §Cancer Immunotherapy Center, Nagoya Kyoritsu Hospital, Nagoya; and ‖Human Health Science, Graduate School of Medicine and Faculty of Medicine, Kyoto University, Kyoto, Japan

Received for publication December 28, 2009. Accepted for publication August 9, 2010.

Address correspondence and reprint requests to Dr. Hiroyasu Ito, Department of Informative Clinical Medicine, Gifu University Graduate School of Medicine, 1-1 Yanagido, Gifu 501-1194, Japan. E-mail address: hito@gifu-u.ac.jp

Abbreviations used in this paper: ALT, alanine aminotransferase; α-GalCer, α-galactosylceramide; IHL, intrahepatic lymphocyte; KC, keratinocyte chemoattractant; KO, knockout; L-Kyn, L-kynurenine; L-Trp, L-tryptophan; MNC, mononuclear cell; 1-MT, 1-methyl-D-tryptophan; WT, wild-type.

www.jimmunol.org/cgi/doi/10.4049/jimmunol.0904173

Materials and Methods

Mice

Male C57BL/6J wild-type (WT) mice (age, 8–10 wk; weight, 25–30 g) were obtained from Japan SLC (Shizuoka, Japan). IDO-knockout (KO) mice with a C57BL/6J background were obtained from The Jackson Laboratory (Bar Harbor, ME). All procedures were conducted in accordance with the National Institutes of Health Guide for the Care and Use of Laboratory Animals, and with the guidelines for the care and use of animals established by the Animal Care and Use Committee of Gifu University.

Animal treatment

α-GalCer was obtained from Funakoshi (Tokyo, Japan) and stored as a 200 μg/ml stock solution in vehicle (0.5% w/v polysorbate-20); it was then diluted in pyrogen-free saline to obtain the indicated dose directly before i.v. injection of a total volume of 200 μl/mouse. Hepatocellular injury was monitored biochemically through measurement of serum alanine aminotransferase (ALT) activity. At appropriate time points, mice were killed by cervical dislocation, and necropsy was performed. Tissue samples were fixed in 10% formalin, embedded in paraffin, and sectioned; the sections were then stained with H&E.

Immunohistochemical analysis

Tissues were fixed in 10% formalin in PBS overnight. Specimens were then embedded in paraffin. Sections that were 4 μm thick were used for H&E staining and immunohistochemical analysis for IDO as described previously (13). For the immunohistochemical analysis, the deparaffinized sections were heated in 0.1 M citrate buffer (pH 6.0), using the Pascal heat-induced target retrieval system (Dako, Carpinteria, CA). Nonspecific Ab binding sites were blocked in PBS (pH 7.4) containing 2% BSA (Wako Pure Chemical Industries, Osaka, Japan) for 60 min. The sections were then incubated with rabbit anti-IDO polyclonal Ab (anti-mouse IDO Ab was generated by the peptide H-CMKPSKKKPTDGDKS-OH) diluted 1/100 in 2% BSA/PBS and incubated overnight at 4°C. The IDO protein was shown by using a labeled streptavidin-biotin kit (Dako Japan, Kyoto, Japan) containing biotinylated Ab and peroxidase-labeled streptavidin. The peroxidase binding sites were detected by staining with 3,3′-diaminobenzidine. Finally, counterstaining was performed using Mayer's hematoxylin.

Determination of L-Kyn concentrations

Plasma from the mice was mixed with 3 volumes of 3% perchloric acid. After centrifugation, the concentrations of L-Kyn in the supernatants were measured using HPLC with a 5-mm octyldecylsilane column (150 × 2.1 mm; Eicom, Kyoto, Japan) and a spectrophotometric detector or a fluorescence spectrometric detector as described previously (13). UV signals were monitored at 355 nm for L-Kyn. The mobile phase consisted of 2.5% acetonitrile in 0.1 M sodium acetate (pH 3.9) and was filtered through a 0.45-μm-pore HA-type filter obtained from Millipore (Bedford, MA). The flow rate was maintained at 0.75 ml/min throughout the chromatographic run.

Analysis of liver transaminase

Hepatocyte damage was assessed at the indicated time points after α-GalCer injection through measurement of plasma ALT activities using an automated clinical analyzer (BM2250; JEOL, Tokyo, Japan).

Hepatic mononuclear cell preparation and flow cytometric analysis

Hepatic mononuclear cells (MNCs) were isolated and purified as previously described (14). Briefly, the excised liver was cut into small pieces with scissors, pressed through a 200-gauge stainless mesh, and suspended in PBS. Lymphocytes were separated from parenchymal hepatocytes and hepatocyte nuclei by Ficoll-Conray (IBL, Gunma, Japan) and washed twice in ice-cold medium. Cell viability and cell numbers were assessed by trypan blue exclusion. For flow cytometry, 2×10^5 liver MNCs were stained using a standard protocol. The following Abs were used: FITC-labeled hamster anti-mouse CD3ε mAb (clone 145-2c11), FITC-labeled rat anti-mouse CD4 mAb (clone RM4-5), FITC-labeled rat anti-mouse Gr-1 mAb (clone RB6-8C5), PE-labeled rat anti-mouse CD49b mAb (clone DX5), PE-labeled rat anti-mouse CD8a mAb (clone 53-6.7), and PE-labeled rat anti-mouse CD11b mAb (clone M1/70) (all from eBioscience, San Diego, CA). Samples were acquired on a FACStar flow cytometer, and data analysis was performed using CellQuest software (BD Biosciences, San Jose, CA).

Isolation of mouse hepatocytes

The abdomen of a sacrificed mouse was opened and a needle was inserted into the vena cava. The portal vein was punctured. The liver was perfused with PBS and liver perfusion medium (Invitrogen Life Technologies, Carlsbad, CA). To obtain nonparenchymal cell populations, the liver was perfused with liver digestion medium (Invitrogen Life Technologies), removed, and gently pressed through a mesh. Nonparenchymal cell were separated from parenchymal hepatocytes by centrifugation at 50 × *g* for 5 min. The purified cell population obtained in the final cell pellet was composed of ≥96% hepatocytes as previously reported (15).

Real-time PCR

Total RNA was isolated and transcribed into cDNA with an RNeasy Mini kit (Qiagen, Hilden, Germany) and High-Capacity cDNA Reverse Transcription kits (Applied Biosystems, Foster City, CA). The resulting cDNA was used as a template for real-time PCR along with primer/probe sets for IDO, TNF-α, IL-2, IL-4, IL-6, IL-10, IFN-γ, MCP-1, MIP-2, keratinocyte chemoattractant (KC), and TGF-β (TaqMan Gene Expression Assays; Applied Biosystems) and 2× TaqMan Universal PCR Master Mix (Applied Biosystems) according to the manufacturer's recommendations. The primer/probe sets for 18S were used as internal controls in the reactions (Applied Biosystems). Real-time PCR data were analyzed using sequence detector software (Applied Biosystems).

Western blot analysis

Protein (20 μg) from the cell lysate was subjected to SDS-PAGE and transferred to nitrocellulose membranes. After blocking nonspecific reactions with 5% skim milk, the membrane was incubated with anti-IDO and anti-GAPDH Abs for 60 min at room temperature and subsequently incubated with peroxidase-labeled anti-mouse or -rabbit IgG Ab for 60 min at room temperature. Immunoreactive protein bands were visualized with ECL Plus (GE Healthcare, Buckinghamshire, U.K.).

Cytokine and chemokine detection by ELISA

The concentrations of circulating TNF-α, IL-6, MIP-2, and KC in the sera were determined by an ELISA kit (R&D Systems, Minneapolis, MN), according to the manufacturer's instructions. The experimental results are expressed as the mean of triplicates (±SD) of three independent experiments.

Intracellular cytokine staining

For intracellular staining, hepatic MNCs from the mice that were administered α-GalCer were incubated for 4 h with brefeldin A (10 μg/ml). Then these cells were fixed, permeabilized with the Cytofix/Cytoperm buffer (BD Pharmingen, San Diego, CA), and stained with FITC-conjugated anti-mouse TNF-α (clone MP6-XT22; eBioscience). Samples were acquired on a FACStar flow cytometer, and data analysis was conducted using the CellQuest software (BD Biosciences).

Statistical analysis

Values are expressed as means (SEM). Differences between the experimental and control groups were analyzed by the Kruskal-Wallis test followed by the Scheffé *F* test. Significance was established at $p < 0.05$.

Results

Upregulation of IDO expression and activity in the liver after α-GalCer injection

We studied the increase in IDO in the liver as a result of α-GalCer treatment. As shown in Fig. 1*A*, to assess the changes in IDO activity in the WT and IDO-KO mice treated with α-GalCer, we first investigated the time course of changes in the serum L-Kyn concentration. The serum L-Kyn levels in WT mice were significantly increased at least as early as 20 h following α-GalCer (2 μg/mouse) injection compared with those in IDO-KO mice, and this increase in serum L-Kyn levels persisted on day 7 after α-GalCer injection. We next examined both IDO mRNA expression and IDO protein levels in the liver of WT and IDO-KO mice administered α-GalCer (Fig. 1*B–D*). IDO mRNA expression in the liver of WT mice was significantly increased at 24 h after α-GalCer injection. Western blot analysis and immunohistochemical examination revealed that the IDO protein levels in the livers from WT mice were upregulated

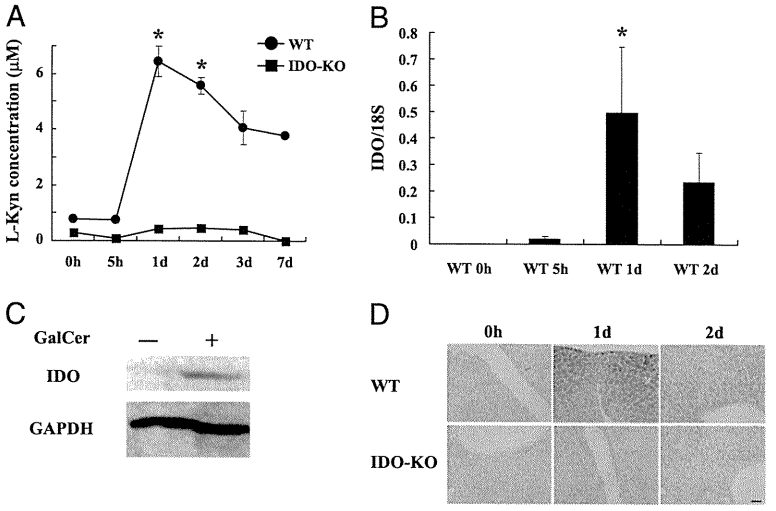

FIGURE 1. Upregulation of IDO expression and activity in the liver after α-GalCer injection. *A*, L-Kyn concentrations in serum determined by performing the HPLC method on WT and IDO-KO mice treated with α-GalCer. Each value is represented by the mean (SEM) of three mice. $*p < 0.05$. *B*, The relative expression levels of IDO mRNA in the livers of WT mice administered α-GalCer were measured using quantitative real-time PCR. The results were normalized by the expression of 18S mRNA. Each value is represented by the mean (SEM) of three mice. $*p < 0.05$. *C*, Expression of IDO protein in the livers of WT mice 1 d after treatment with α-GalCer was examined by Western blot analysis and was determined using the GAPDH protein. Data are representative of at least three independent experiments with similar results. *D*, Immunohistochemical analysis of IDO in the liver of WT and IDO-KO mice after α-GalCer injection. IDO protein was stained by using a labeled streptavidin-biotin kit containing biotinylated Ab and peroxidase-labeled streptavidin. The peroxidase binding sites were detected by staining with 3,39-diaminobenzidine. Scale bar, 25 μm. Original magnification ×200. Data are representative of at least three independent experiments with similar results.

after α-GalCer injection. This increase in IDO expression was observed in hepatocytes in particular.

Induction of liver injury by α-GalCer in WT mice and IDO-KO mice

To determine whether IDO plays a critical role in α-GalCer–induced liver injury, IDO-KO mice and WT mice were i.v. injected with α-GalCer (2 μg/mouse). Serum ALT activity started increasing at 12 h, reached a peak at 1 d, and returned to normal at 5 d after injection in WT mice (Fig. 2*A*). Surprisingly, serum ALT activity in IDO-KO mice significantly increased at 1 and 2 d after the injection compared with the activity in WT mice. To examine histological changes in the liver in the presence or absence of IDO after α-GalCer injection, we subjected liver tissues to H&E staining. As shown in Fig. 2*B*, livers from both WT and IDO-KO mice were mostly histologically normal except for a few very small and widely scattered necroinflammatory foci consisting of lymphomononuclear cells and apoptotic hepatocytes 1 d after α-GalCer injection. At 2 d after α-GalCer injection, the necroinflammatory foci in the livers of IDO-KO mice became larger and more abundant compared with those in WT mice, consisting of a mixed population of lymphomononuclear cells and apoptotic hepatocytes that often displayed granulomatous features in the hepatic parenchyma.

α-GalCer–induced TNF-α production in WT and IDO-KO mice

It was previously reported that neutralization of TNF-α significantly reduced induced α-GalCer–induced hepatic injury (12); in fact, TNF-α is thought to play a critical role in α-GalCer–induced liver injury. Therefore, we next examined TNF-α production in WT and IDO-KO mice treated with α-GalCer. TNF-α mRNA expression in the livers of IDO-KO mice was increased compared with that in the livers of WT mice at 12 h after α-GalCer treatment (Fig. 3*A*). Moreover, we measured plasma TNF-α levels up to 2 d after administration of 2 μg of α-GalCer to WT and IDO-KO mice by ELISA (Fig. 3*B*). The TNF-α levels peaked at 5 h after α-GalCer application in both WT mice and IDO-KO mice. How-

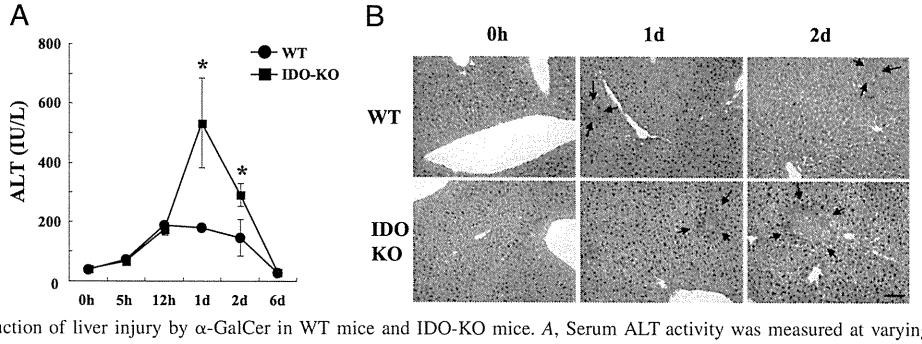

FIGURE 2. Induction of liver injury by α-GalCer in WT mice and IDO-KO mice. *A*, Serum ALT activity was measured at varying time points after α-GalCer injection into WT and IDO-KO mice. Each value is represented by the mean (SEM) of three mice. $*p < 0.05$. *B*, Histopathological characteristics of WT and IDO-KO mice livers observed at 0, 1, and 2 d after α-GalCer administration in these mice. H&E, original magnification ×200; scale bar, 100 μm. Arrows designate necroinflammatory foci in the liver. These experiments were repeated three times, and the same results were obtained.